To the Graduate Council:

I am submitting herewith a dissertation written by Dwayne John entitled "Nuclear Modification Factor (R_{AA}) in $\sqrt{s_{NN}} = 200$ GeV $Cu + Cu$ Collisions at Forward Rapidity." I have examined the final electronic copy of this thesis for form and content and recommend that it be accepted in partial fulfillment of the requirements for the degree of Master of Science, with a major in Physics.

Ken Read, Major Professor

We have read this dissertation
and recommend its acceptance:

Soren Sorensen

Yuri Efremenko

Accepted for the Council:

Carolyn R. Hodges, Vice Provost
and Dean of the Graduate School

(Original signatures are on file with official student records.)

Nuclear Modification Factor (R_{AA}) in $\sqrt{s_{NN}} = 200$ GeV $Cu + Cu$ Collisions at Forward Rapidity

A Thesis

Presented for the

Master of Science

Degree

The University of Tennessee, Knoxville

Dwayne John

May 2009

Dedication

To my ancestors, this is for who paved the way.

Acknowledgments

Abstract

Relativistic heavy-ion collisions are an integral component in studying the small-scale structure of the universe and a probe for nuclear processes. Measurements are an important part of confirming any theory that plans to accurately describe the fundamental processes of the universe. One such measurement of these interactions is the Nuclear Modification Factor (R_{AA}).

This thesis presents the measurement of R_{AA} as a function of transverse momentum for hadrons in $Cu + Cu$ collisions at forward angles. The experiment was performed with the Relativistic Heavy Ion Collider (RHIC) at Brookhaven National Laboratory (BNL) from data recorded in 2005 by the PHENIX collaboration. A new analysis technique was developed to measure forward angle stopped hadron yields in Gap 3 of the PHENIX Muon Identifier. The yield of the stopped hadrons is measured and is used to calculate R_{AA}.

Contents

List of Figures

List of Tables

Chapter 1

Introduction

1.1 Organization

This thesis is organized as follows: the first chapter is a brief introduction to the overall field of particle physics along with a motivation behind the experiment and analysis; the second chapter includes a description of the experimental apparatus and its various components; the third chapter gives a theoretical introduction to the measurement being calculated and how it is derived; chapter four discusses how the analysis is executed; and chapters five and six lend a discussion of the results obtained and how they compare to similar measurements in the field.

1.2 Heavy-Ion Physics

Germaine Williams once said, "To create a universe all I need is 1,000 trillion degrees, sodium 22, betatrons in the cloud chamber, keep the noise down so I don't arouse my neighbors." This may seem absurd to most at first glance but this is to some extent what particle physicists at Brookhaven National Laboratory (BNL) are trying to achieve. They are recreating miniature big bangs repeatedly with the particle accelerator in an attempt at observing the reproduction of one part of the creation puzzle, the quark hadron transition [1]. In this chapter there will be a discussion of the standard model of particle physics, the quark-gluon plasma, and the motivation for studying nuclear modification which is discussed in the last section of this chapter.

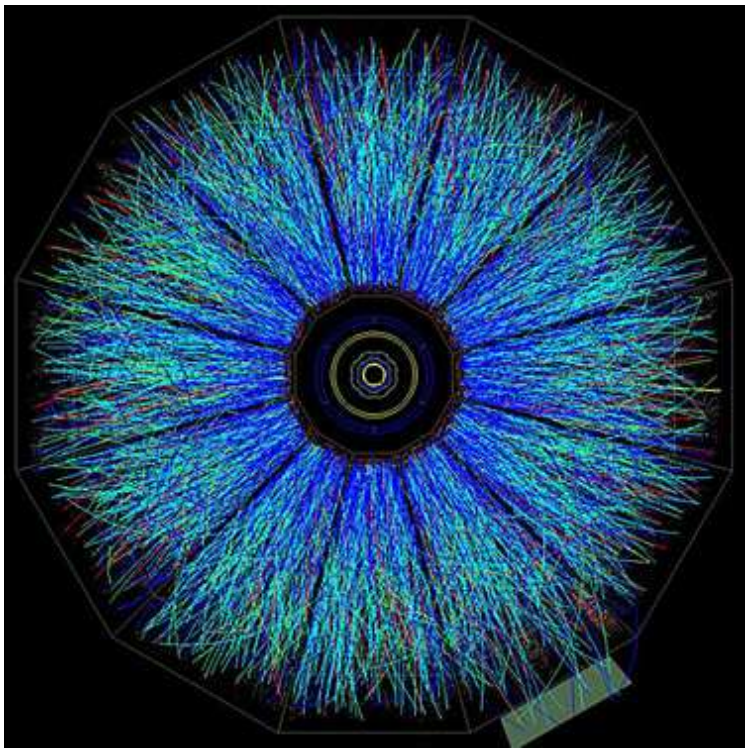

Figure 1.1: The different colors represent different particle tracks in the STAR detector.

Heavy-ion physics experiments produce many particles in just one collision as seen in Figure 1.1. This representation of particle tracks in the STAR detector shows just how violent a single collision is. Measuring the products of these collisions (200 GeV $Au + Au$) helps us verify the standard model of particle physics.

The Standard Model of Elementary Particle Physics describes three of the four fundamental interactions: electromagnetism, the weak and the strong nuclear force. The strong force is described by the theory of Quantum Chromodynamics (QCD). In this model there are two sets of particles: fermions which have half-integer spin and bosons that have whole-integer spin. The fermions can then be divided into quarks and leptons and are classified in three generations.

Quarks are elementary particles that have a spin of $\frac{1}{2}$ that cannot be observed as free particles [2]. Instead, quarks are bound to other quarks by the strong nuclear force via gluons to form normal nuclear matter called hadrons (mesons and baryons). These particles (hadrons) are most commonly seen in nature as protons and neutrons. Hadrons make up the largest amount of particles that are created from heavy-ion collisions.

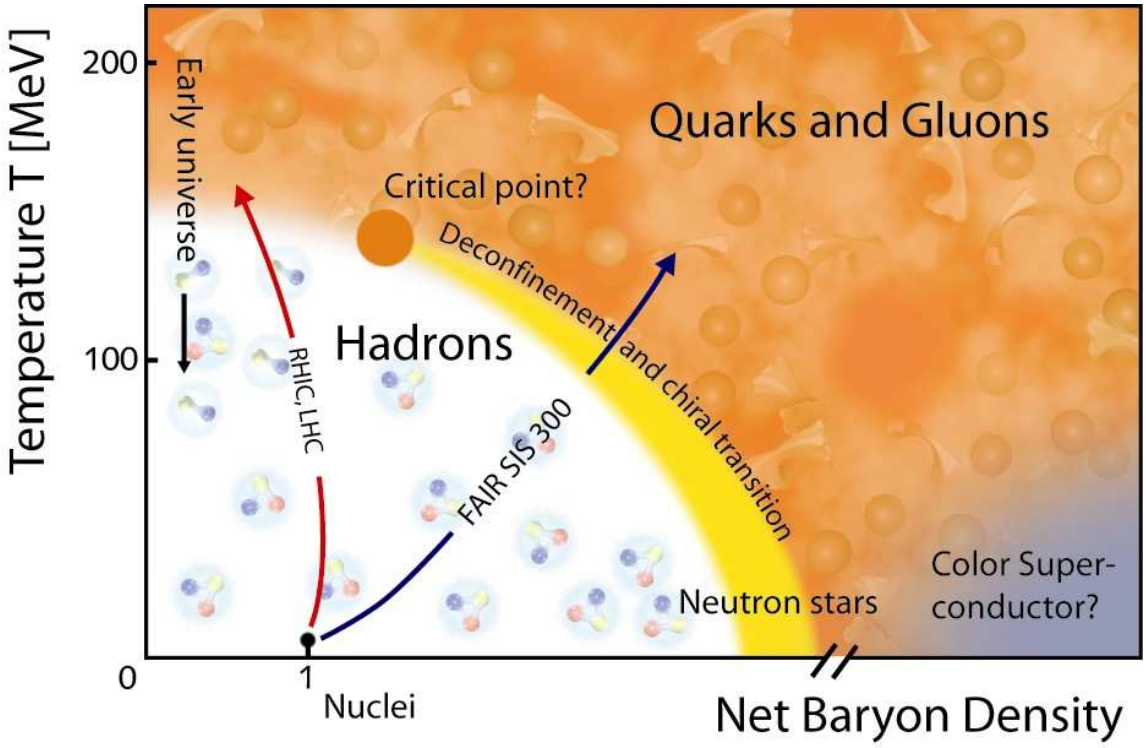

Figure 1.2: The Phase Diagram of the Quark-Gluon Plasma. The y-axis is the temperature in MeV and the x-axis is in units of normal nuclear matter density. [3]

Figure 1.2 is a notional phase diagram in which nuclear matter in a high energy nuclear collision follows the trajectory of the arrows. If baryon density or the temperature is increased far enough, there is a phase transition to the Quark-Gluon Plasma, where quarks and gluons are unconfined. Low energy colliders such as FAIR [4] are expected to demonstrate this in the future. RHIC accomplishes this by increasing the temperature of the nuclei through high energy collisions. Baryon density, however, is low at RHIC. It is believed that the early universe was once a Quark Gluon Plasma and transitioned down into normal nuclear matter. In Figure 1.2, this is where the baryon density is very low.

The Quark Gluon Plasma (QGP), is a dense fluid medium thought to have existed several microseconds after the Big Bang [1]. There were many phase transitions after the Big Bang: Grand Unification Transition (10^{-35} s), Electro-weak transition (10^{-11} s), and the earliest measurable quark hadron transition, the QGP, which occurred at 10^{-6} s. Studying the QGP reveals more information about the origins of the universe. It is a phase that is predicted by QCD where quarks and gluons are no longer bound to each other in pairs or triplets, in contrast to nuclear matter where quarks are confined to each other [5].

In a generic electromagnetic plasma, the temperature is high so that electrons are freed from atoms by breaking the electromagnetic bonds to form a mixture of electrons and ions. Since the strong nuclear force is the most powerful of all the fundamental interactions, it takes an exorbitant amount of energy to reach a sufficiently high temperature and pressure to create a plasma from heavy ions (QGP). The temperature of an electromagnetic plasma is only on the order of a few electron-volts. The Quark-Gluon Plasma is analogous to a generic plasma in the sense that when the temperature of normal nuclear matter is increased to 170 MeV [6], the quarks are deconfined by breaking free from the strong nuclear force inside the hadrons to form a mixture of free quarks and gluons.

Apart from its brief lifetime, the characteristics such as high temperature and high pressure of the plasma is what makes the QGP very challenging to study. It is very difficult to recreate such energies in the laboratory for a small volume for such a short time but collisions of heavy ions at the Relativistic Heavy Ion Collider (RHIC) are thought to produce the conditions needed to produce a QGP [1].

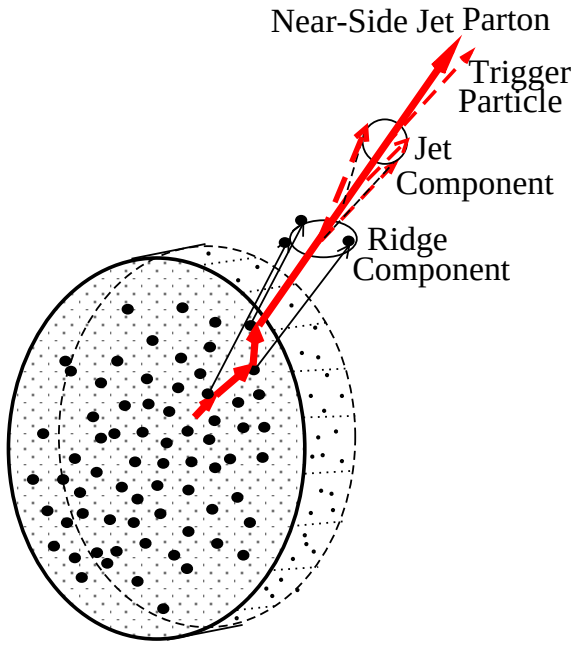

Figure 1.3: Schematic representation of a near-side jet parton represented by adjoining thick arrows. Occurs in a dense medium whose partons are represented by solid circle points.

1.3 Motivation

If the same processes that were functioning in generic heavy ion $A + A$ collisions are also ongoing in $p+p$ collisions, then one can predict the yield of high-p_T (transverse momentum) hadrons in these collisions since the number of equivalent $p + p$ collisions for an $A + A$ collision is straightforward to calculate. At $p_T > 3.0$ GeV/c in central (0 - 10% overlap of particles in the reaction plane) $A+A$ collisions, the yield of hadrons created at mid-rapidity was observed to be much lower than this expectation by a factor of 5 [7]. The ratio between the observed and exptected yield is defined as R_{AA}. So an R_{AA} of less than 1.0 is typically characterized as suppression.

In elementary high energy $p + p$ collisions the largest source of hadrons at high transverse momentum (p_T) is jet fragmentation. Jet fragments are gluons or light quarks that experience hard scattering (scattering into a state of high, transverse momentum greater than a few GeV/c) and then "fragment" into "jets" of high p_T hadrons.

Jets are narrow cones of hadrons and other particles produced by the hadronization (fragmentation) of a quark or gluon in a heavy ion experiment collision. A pictorial example

of these jets is shown in Figure 1.3. Jets are produced in nucleon-nucleon collisions and interact with the dense medium produced in the interacting region.

The strong weakening of the away-side jet in its transition through the produced dense parton matter is one of the many notable experimental observations in relativistic heavy-ion collisions and is a signature for the production of the strongly coupled quark-gluon plasma [8].

The most commonly assumed mechanism for the large hadron suppresion is that the hard-scattered parton (gluon or light quark) interacts strongly losing energy with the medium created in the volume of the whole $A + A$ collision. Very strong suppression is then evidence that the medium created at RHIC is dense. To examine the effect systematically one could change the medium's density while maintaining its transverse geometry. One way to perform this is to examine spectra at forward angles. Particles studied at forward angles coincide with sources at high rapidity. In the Bjorken picture of the initially thermalized state of an $A + A$ collision, there is a close correlation between rapidity and physical position.

Rapidity (y) is defined as

$$y = \frac{1}{2} ln \frac{E + p_z}{E - p_z} \tag{1.1}$$

where p_z is the longitudinal momentum and E is the energy.

Another important and useful variable discussed later in this thesis, pseudorapidity, η is

$$\eta = -ln[tan(\frac{\theta}{2})] \tag{1.2}$$

where θ is the angle between the particle momentum p and the beam axis.

The lower rapidity density of final-state particles dN/dy (or transverse energy dE_T/dy) observed at higher rapidity y suggests a lower spatial energy density in the medium at the corresponding position. BRAHMS has measured R_{AA} for hadrons at forward rapidities (see Figure 1.4) and has found that for pions the suppression does not change at all with rapidity even though the energy density in the Bjorken picture is decreased by a factor of 3. Studying this important and puzzling result is worth investigating with PHENIX detector [7].

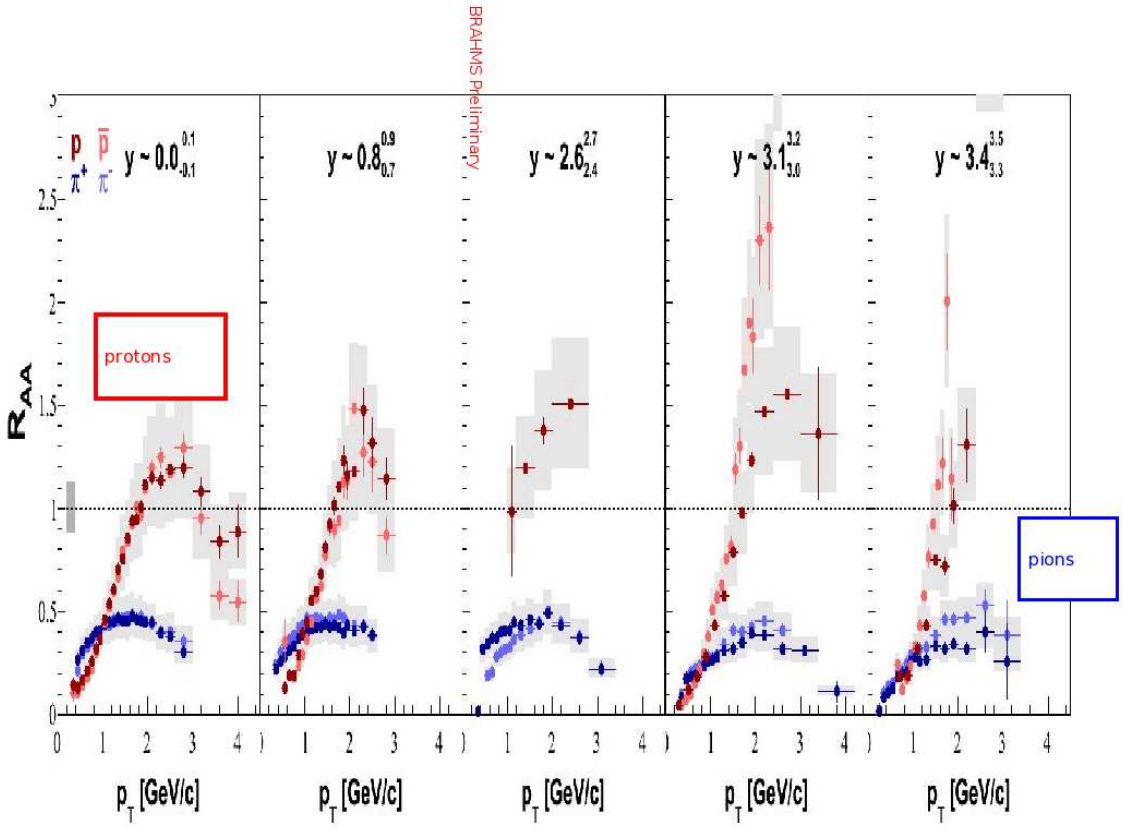

Figure 1.4: The nuclear modification factor R_{AA} for protons (red) and pions (blue) at different rapidities, as measured by BRAHMS in central $Au + Au$ collisions $\sqrt{s_{NN}} = 200$ GeV. The modification for the mesons (i.e. pions) shows very little dependence on rapidity.

Chapter 2

The Experiment

This chapter will review the experimental apparatus which includes the (RHIC) Relativistic Heavy-Ion particle accelerator, the PHENIX experiment, and the specific PHENIX subsystem detectors used to perform the measurement presented in this thesis.

2.1 RHIC

RHIC is located at Brookhaven National Laboratory (BNL), on Long Island, New York. RHIC was built next to the existing Alternating Gradient Synchrotron (AGS) accelerator complex which is now an injector to RHIC. The PHENIX detector measures the collision products.

RHIC was constructed for the main purpose of studying the QGP and is designed to create new particles by colliding relativistic ions together close to the speed of light, c (3.0×10^8 m/s). These relativistic collisions which occur at RHIC are analogous to mini big bangs that are occuring repeatedly. RHIC has the unique ability of colliding the many species of nuclei from $p + p$ to $Au + Au$ over a wide range of collision energies. These energies range from a minimum center of mass energy per nucleon-nucleon ($N + N$) of $\sqrt{s_{NN}} = 22$ GeV to a maximum of $\sqrt{s_{NN}} = 200$ GeV for $Cu + Cu$ whereas the maximum $\sqrt{s_{NN}}$ for $p + p$ is 500 GeV.

The following summarizes existing material from a colleague's thesis [9]. RHIC generates collisions with two seperate super-conducting rings (blue and yellow) with a cir-

cumference of 3.8 km. Each ring has it's own source of ions, one clockwise and the other counter-clockwise, which allows collisions of unlike ion species to occur. Also, two separate Van de Graaf generators function as the first stage of acceleration of heavy ions. The ions are acquired from the proton linear accelerator, or LINAC.

Copper ions are created from the pulsed sputter ion source at the front of the Tandem Van de Graaff. The ions are partially stripped of electrons with a foil and are accelerated to an energy of 1 MeV per nucleon by the time they exit the Van de Graaff. The copper beam navigates up the transfer line to the Booster Synchrotron which accelerates the ions to an energy of 95 MeV per nucleon. The ions depart from the Booster Synchrotron and pass through the stripper, which removes the ions. The ions are then injected into the AGS in bunches, strings of ions 30 cm long with thickness of an average human hair, and accelerated to the RHIC injection energy of 10.8 GeV per nucleon. The ions are then rebunched into smaller bunches in the AGS and then navigated through another electron stripper in the AGS-to-RHIC Beam Transfer Line.

Afterwards, the ions undergo another injection into the RHIC rings one bunch at a time and are accelerated to a maximum energy of 100 GeV per nucleon in the accelerator rings. The RHIC magnets are superconducting and must be cooled to a temperature of 4.6 Kelvin and are properly phase adjusted (referred to as cogging) to successfully steer the ion beams around the rings for collisions to occur at the proper interaction points of the different experiments. The bunches now actually cross 10,000,000 per second, however, the rate of $Cu + Cu$ collisions is 10 kHz [6].

When RHIC recorded its first collisions in 2000, the four detectors that functioned were BRAHMS, PHENIX, PHOBOS, and STAR. The experimental collaborations extract measurements by measuring particles that are ejected from the collisions. PHENIX resides at the 8'oclock position on the ring as seen in Figure 2.1.

2.2 PHENIX

PHENIX, or the Pioneering High Energy Nuclear Interaction eXperiment, is the largest experimental collaboration of the four experiments that ever functioned at RHIC (Fig. 2.2). The PHENIX experiment studies the high energy collisions of heavy ions. The PHENIX

Figure 2.1: God's eye photograph of the RHIC complex [10].

detectors record the most collisions of all the detectors at RHIC and are designed to measure products of these collisions.

2.3 The PHENIX Detector

The PHENIX detector which is used for the measurements in this thesis does not cover the full 4π solid angle and consists of a set of global event detectors and four spectrometer arms, with each pair of spectrometer arms providing a specific set of physics observations. Measurements are made by the pair of spectrometers measuring electrons, photons and hadrons which covers one primary kinematic region referred to as mid-rapidity, while a second pair of spectrometers measures muons at another primary kinematic region, forward rapidity. The magnetic field in the collision area of the PHENIX detector is axial and the magnets of the muon arms create a radial magnetic field. The PHENIX detector is made up of (many) independent subsystems working simultaneously while using other electronics to better identify particles.

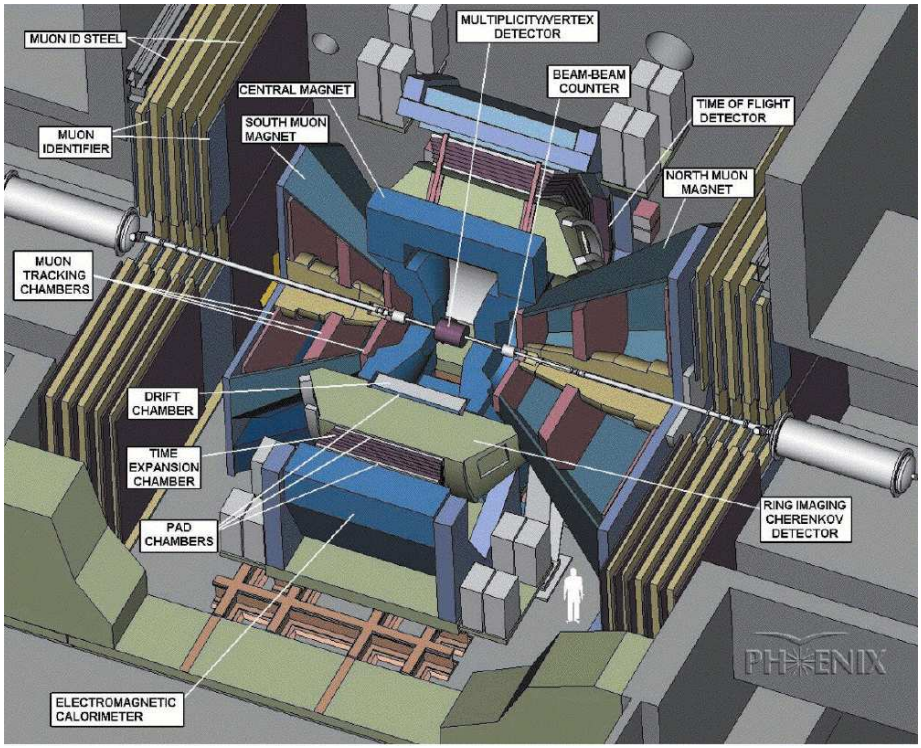

Figure 2.2: Schematic diagram of the PHENIX detector.

2.4 Beam-Beam Counter

The BBC determines the start of timing for the Time-of-Flight measurement, provides a level-1 trigger signal of nuclear interaction, and can also determine the centrality of a collision when combined with a ZDC in formation. The BBC is designed to function in both $p + p$ and heavy ion collision settings.

The BBC can also be used to measure the interaction vertex with a resolution for $p+p$ collisions of about 2 cm and 0.5 cm for $Au + Au$ collisions. It also provides the start time of the event and allows for selection of beam crossings. Since there are significantly more heavy ion collisions than the detector can register, the minbias trigger records specific trigger events based upon an explicit criteria for which events are selected.

The results for this analysis are for minimum bias triggered collisions. The BBC is located 1.44 m away from the point of collision and the pseudorapidity coverage for the BBC is roughly ± 3.1 to ± 3.9. It can be positive or negative. The BBC measures approximately 55% of total inelastic cross section for $p + p$ collisions [11].

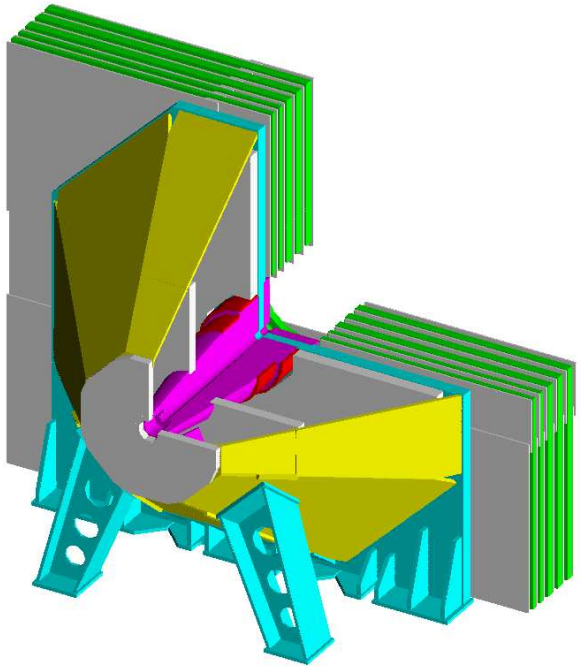

Figure 2.3: Schematic diagram of the Muon Tracker.

2.5 The Muon Tracker (MuTR)

The Muon Tracker measures the momentum of the particles by making precision position determinations inside a magnetic field. The MuTR (north and south) are shaped like octants and are made up of three stations (separated along the z-axis) of cathode-strip readout tracking chambers mounted inside conical-shaped muon magnets. The MuTR is shown in Figure 2.3. These magnets have multiple cathode strip orientations and readout planes in each station.

Tracking station 1 chambers are placed closest to the interaction point and are the smallest. Their radius from inside to outside is 1.25 m. The thickness of the tracking station 2 detector is required to be $\leq 0.1\%$ of a radiation length in order to maintain a good momentum resolution down to 1.5 GeV. Tracking Station 3 chambers are the biggest of the three tracking chambers. Each octant chamber is roughly 2.4 m long and 2.4 m wide.

2.6 The Muon Identifier (MuID)

The MuID is the other important component of the PHENIX Muon Arm. After a charged particle goes through Station 3 of the MuTR it must then pass through five layers of steel absorbers alternating with layers of sensitive volumes (sensitive gas detectors). The sensitive volumes record the passage of particles in two orthogonal directions. In other words the sensitive volumes allow the reconstruction of the two dimensional location of the particle with 8 cm precision in that layer. The steel absorber plates will preferentially absorb hadrons. Therefore, the MuID allows muon-hadron separation.

Since muons are vastly outnumbered by hadrons, a strategy is needed to separate them. This thesis takes advantage of the fact that even though the MuID is designed to eliminate hadrons, with a clever technique described in Section 4.6, it can be used to select a clean sample of hadrons although it cannot identify which species of hadrons.

Dividing the absorber into multiple layers improves the measurement of the particle trajectories in the MuID. It is to the experiment's greatest advantage to make sure the early absorber layers are divided more finely to increase the acceptance for particle detection. The MuID is divided into a total of four steel absorbers after the 30 cm thick muon magnet backplate of the north arm with thicknesses 10, 10, 20, and 20 cm. The five gaps in the middle of the absorbers are fitted with MuID instrumentation placed within the panels. The MuID south arm is virtually identical save for the muon magnet backplate which is only 20 cm in thickness but it resides at the same distance from the interaction point of the collision.

2.7 Central Arms

A thorough report on the PHENIX Central Arms can be located in the following literature. The PHENIX central arms data are shown in Figure 2.4 [12, 13].

2.8 Track Reconstruction

The first step in the reconstruction is to process the raw data to get hit positions in the different stations in the Muon Tracker and the different gaps in the MuID. The next step

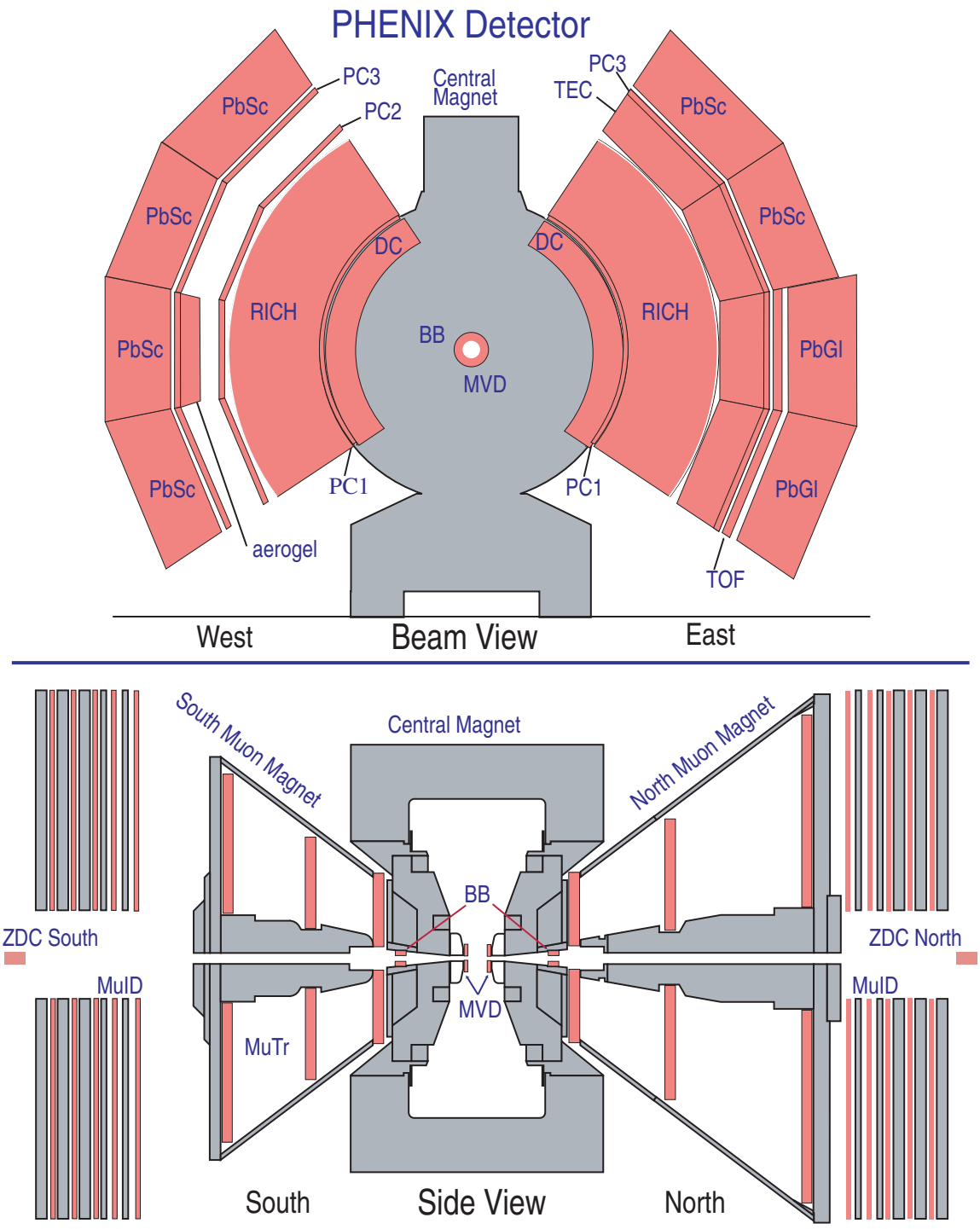

Figure 2.4: This diagram shows the Muon ID.

is to collect those hits into likely groupings that belong to a particle trajectory.

Using undergraduate physics principles of electromagnetism such as the Lorentz force law, the MuTR measures momentum of charged particles using the formula $p = qBr$ where q is the charge of the particle, B is the magnetic field of the muon magnet the particle passes through in the detector, and R is the radius. The radius is reconstructed by measured hits on the three stations for which reconstruction of tracks occur. The MuTR takes this information along with trajectory data and calculates the momentum of each track. The momentum is vital to the analysis because histograms used in results are binned with respect to p_T.

By observing measurements at the last gap collected in the trajectory, the last gap is then identified. By combining the information about the selected particles with the last gap (not deepest gap), cut on the momentum and can properly obtain a clean sample of hadrons. A discussion of this can be found in Chapter 4.

Chapter 3

Nuclear Modification in $Cu + Cu$

The Nuclear Modification factor, R_{AA}, is one of many variables used to probe the QGP. By measuring R_{AA}, one can study properties of the QGP and characterize the produced nuclear matter.

3.1 Introduction: The Glauber Model

The Glauber Model is used in relativistic heavy ion physics to calculate geometric quantities, which are usually impact parameter $\vec{b}$, number of participating nucleons (N_{part}), and the number of binary nucleon-nucleon collisions (N_{coll}). These geometric attributes of high-energy heavy-ion collisions are important in collision dynamics.

As shown in Figure 3.2, $\vec{b}$ is the transverse distance between the centers of two colliding nuclei. Heavy-ion collisions with a small $\vec{b}$ and large overlap are called central collisions. Collisions with large $\vec{b}$ and small overlap are called peripheral collisions. This value of $\vec{b}$ and overlap defines the centrality of the collision.

Collision dynamics of nucleus-nucleus collision processes are most usefully described by considering the collision at the parton level. Once an incident projectile nucleon undergoes a collision, the resultant baryonic product can be treated as a projectile which continues to make collisions with other particles in the same direction of the projectile. The mean-free path of an elementary baryon-baryon collision can be estimated. Although a baryon of a particular nucleus can become excited and have a different cross section, σ, when it egresses

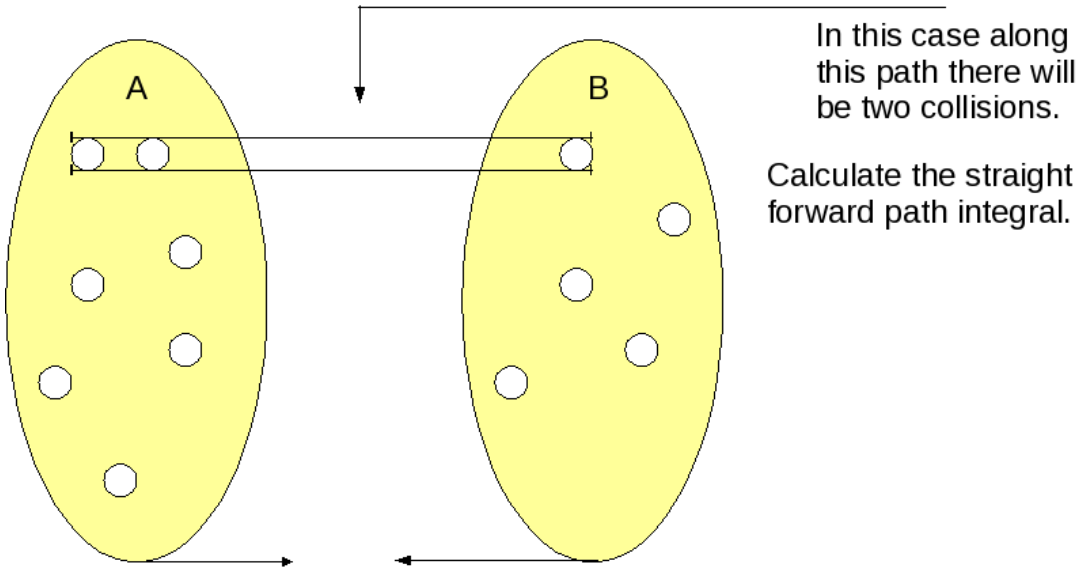

Figure 3.1: A typical $A + A$ collision.

through the other nucleus, the Glauber model is simplified by assuming the baryon-baryon cross sections are the same. [14]

The thickness function for nucleus A is

$$T_A(\vec{b_A}) = \int \rho_A(\vec{b_A}, z_A) d\vec{b_A} dz_A \tag{3.1}$$

and the thickness function for nucleus B is

$$T_B(\vec{b_B}) = \int \rho_B(\vec{b_B}, z_B) d\vec{b_B} dz_B \tag{3.2}$$

The thickness function with respect to impact parameter $\vec{b}$ for the collision of nucleus B on nucleus A is $T(b)$, where ρ is the usual number density function divided by the number of baryons in the nucleus. Convoluting T_A and T_B along with the function t yields the following equation:

$$T_{AB}(\vec{b}) = \int \rho_A(\vec{b_A}, z_A) d\vec{b_A} dz_A \cdot \rho_B(\vec{b_B}, z_B) d\vec{b_B} dz_B t(\vec{b} - \vec{b_A} + \vec{b_B}). \tag{3.3}$$

The probability of finding a baryon in the volume element $d\vec{b}d\vec{z}$ in nucleus A at position

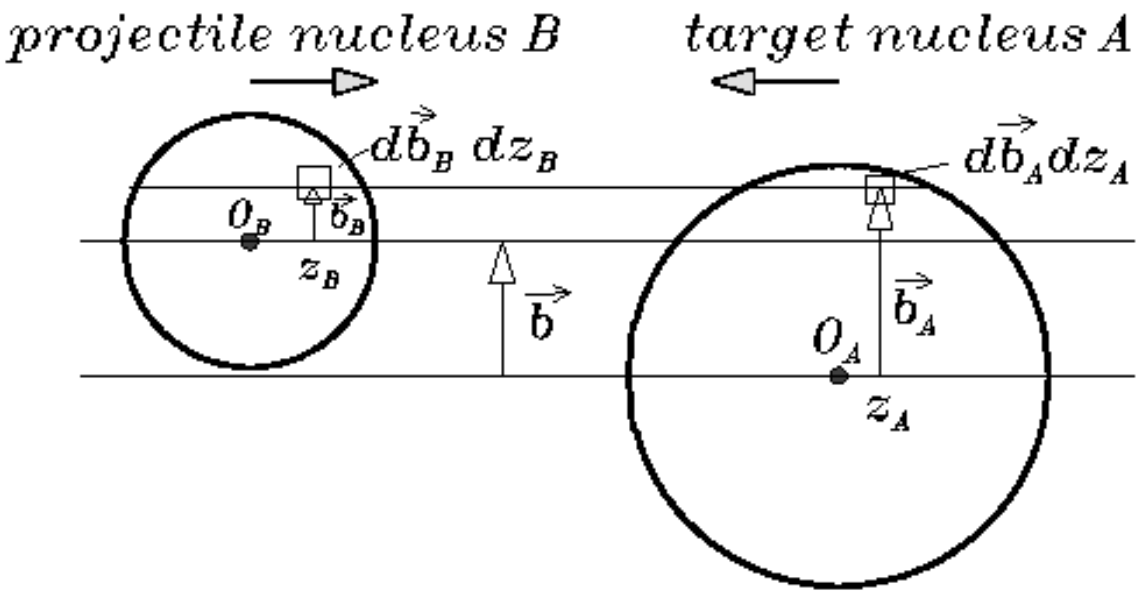

Figure 3.2: Collision of the projectile nucleus B with target nucleus A at impact parameter $\vec{b}$. The circles represent nuclei. [15]

(b, z) is $\rho_A(b_A, z_A)db_A dz_A$. Another probability that needs to be taken into account is the probability of having a baryon-baryon collision within the transverse area element $d\vec{b}$. It is labeled t and arises geometrically when one baryon is situated at an impact parameter $\vec{b}$ relative to another baryon. We can write the number of nucleons in a tube through the nucleus at a distance b_A from the center of the nucleus. Note that $\vec{b_A} - \vec{b_B} = \vec{b}$ and the superscript NN refers to the fact that we are dealing with nucleon-nucleon collisions. In order to calculate the number of nucleons in tube A and tube B respectively, multiply the number of nucleons in the nucleus $\times$ the thickness function $\times$ the cross section of the baryon σ.

$$Nucleons\ in\ tube\ A = A \cdot T_A(\vec{b_A})\sigma_{in}^{NN} \tag{3.4}$$

$$Nucleons\ in\ tube\ B = B \cdot T_B(\vec{b_B})\sigma_{in}^{NN} \tag{3.5}$$

By multiplying the number of nucleons in tube A $\times$ tube B we can effectively calculate the number of binary collisions.

$$N_{coll} = A \cdot T_A(\vec{b_A})\sigma_{in}^{NN} B \cdot T_B(\vec{b_B})\sigma_{in}^{NN} \tag{3.6}$$

N_{coll} is essential in scaling $p+p$ collisions with $Cu+Cu$ collisions in order to caclulate an accurate R_{AA} measurement [15].

3.2 Nuclear Modification Factor, R_{AA}

The nuclear modificatiion factor, R_{AA} for heavy ion collisions is

$$R_{AA} = \frac{dN_{A+A}}{< N_{coll} > \times dN_{p+p}} \tag{3.7}$$

which is a quantifier of the QGP and its effects on particle yields. R_{AA} is the ratio of corrected particle yields for heavy ion collisions divided by naively scaled $p+p$ collisions. An uncorrected invariant yield is defined as

$$Y_{A+A} = \frac{N_{A+A}}{2\pi p_T d\eta dp_T} \tag{3.8}$$

The corrected invariant yield dN_{A+A} represents the yield for the heavy ion species being collided,which in the case of this analysis, is $Cu+Cu$. The denominatory dN_{p+p} represents binary nucleon-nucleon collision particle yields. The scaling factor $< N_{coll} >$ is mentioned above and differs according to the centrality class of the collisions in question. In this thesis, $< N_{coll} >$ may be used interchangeably with $< N_{bin} >$.

Table 3.1: Values of N_{part} and the number of binary parton-parton collisions for $Cu + Cu$ for the given centralities.

$Cu + Cu$		
Centrality	$< N_{coll} >$	N_{part}
Minimum Bias	52.3	34.6
0-20%	151.8	85.9
20-40%	61.6	45.2
40-94%	50	60

Chapter 4

Analysis of Nuclear Modification in the PHENIX Muon Arms

4.1 Overview

The methodology and analysis for the measurement of the Nuclear Modification Factor, R_{AA}, of unidentified stopped charged hadrons in the PHENIX MuID is presented in this chapter. This measurement is extracted from tracks detected by the muon arms from $Cu+Cu$ and $p+p$ collisions for Run 5 (2005) at RHIC. The mix of unidentified measured charged hadrons is studied by simulations: they are primarily pions, kaons, and to a much lesser extent, protons, and anti-protons [16]. Track selection, or applied cuts (defined later in the chapter) for data and simulations are calculated separately for $Cu+Cu$ and $p+p$.

The R_{AA} measurement for this analysis is calculated operationally in the following equation.

$$R_{AA}(p_T) = \frac{Y_{A+A}}{< N_{coll} > Y_{p+p}} \tag{4.1}$$

The final result for the analysis is shown in Figure 4.1. Data for Gap 3 stopped hadrons is determined by applying track selection criteria optimized for shallow gap hadron yields. These track selection criteria are called "cuts." (defined later in the chapter) Only stopped hadrons are needed for this analysis which is a subset of all tracks in data. We start by obtaining the uncorrected invariant yields for $Cu+Cu$ and $p+p$ and construct these ratios. By using ratios the biggest systematic errors cancel. Section 4.2 explains how to obtain

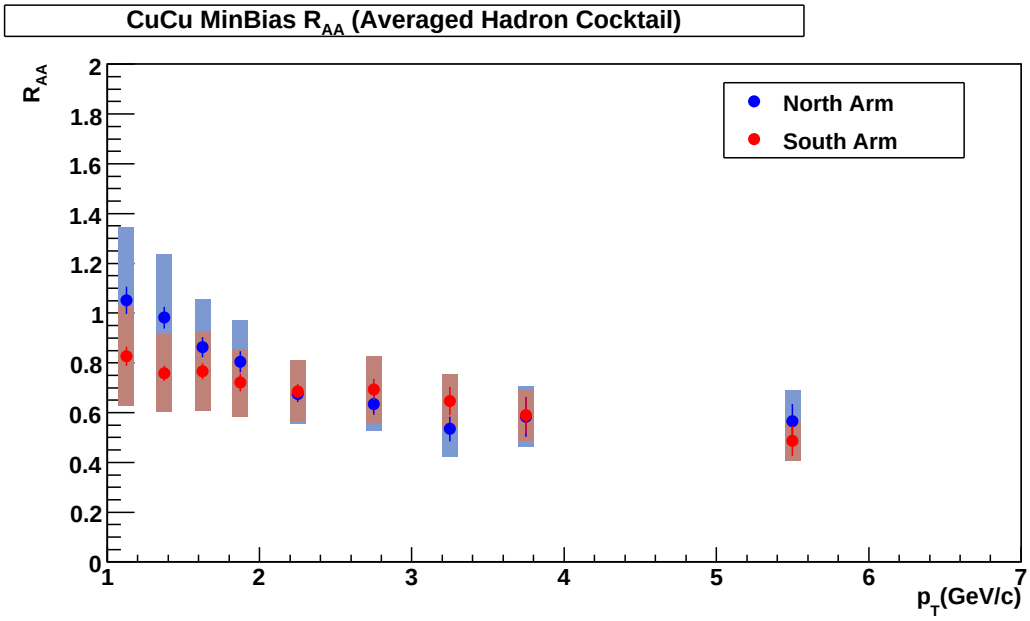

Figure 4.1: Acceptance and efficiency corrected transverse momentum distribution of R_{AA} data for stopped hadrons in Gap 3 of the PHENIX detector separated by north (blue) and south (red) arms using $Cu + Cu$ and $p + p$. The statistical errors are lines and the systematic errors are represented by bands.

the ratio of the uncorrected yields for $Cu + Cu$ and $p + p$. Section 4.3 explains how to obtain the normalized correction. Section 4.4 explains the systematic errors and presents the central values. How the hadrons are obtained is discussed in Section 4.5. Section 4.6 discusses how hadrons are identified in the analysis.

$$R_{AA}(p_T) = \frac{\frac{N_{AA}}{\epsilon_{A+A}}}{< N_{coll} > \frac{N_{p+p}}{\epsilon_{p+p}}} \tag{4.2}$$

$$R_{AA}(p_T) = \frac{N_{AA}\epsilon_{pp}}{N_{coll}^{A+A} N_{pp} \epsilon_{AA}} \tag{4.3}$$

These equations are responsible for producing the final R_{AA} results shown in Table 4.1 and Figure 4.1 and discussed further in Chapter 5. The final result can be seen in Figure 4.1. The rest of this chapter will discuss how the central values and systematic errors are obtained.

4.2 Uncorrected Invariant Yields

The uncorrected invariant yield, N, is defined as the number of particles measured (unidentified charged hadrons in this case) per $p+p$ collision in Gap 3. The transverse momentum distribution of the uncorrected invariant yields are shown in Figures 4.2 and 4.3.

We divide the two distributions of the uncorrected invariant yields shown in the equations below:

$$\frac{N_{Cu+Cu}}{2\pi p_T d\eta dp_T} \tag{4.4}$$

by

$$\frac{N_{p+p}}{2\pi p_T d\eta dp_T}. \tag{4.5}$$

We multiply the denominator by N_{coll} to get an uncorrected R_{AA} value.

4.3 Normalized Invariant Yields

The normalized invariant yields, Y, for $Cu + Cu$ and $p + p$ collisions can be calculated the following way by dividing the number of stopped hadrons n by the number of events. The data used for this experiment is part of the 400 TB of data from Run 5. A total of 1.77 $\times 10^8$ $Cu + Cu$ events were recorded, whereas the PHENIX detector recorded 7.3857 $\times 10^9$ $p+p$ events in the north arm and 7.7163 $\times 10^9$ events in the south arm. Out of those events, a total of 174,233 tracks were selected for $p + p$ collisions. The North Arm Gap 3 1S detected 75,613 of those tracks while the South Arm Gap 3 1S detected 98,620 tracks of the total tracks. These values are used in this section to calculate a normalized R_{AA}.

By defining $norm_{Cu+Cu} \equiv 1.77 \times 10^8$ and $norm_{p+p} \approx 7.3857 \times 10^9$, a normalized R_{AA} is calculated by Eq. 4.6.

$$R_{AA}(p_T) = \frac{\frac{n_{Cu+Cu}}{norm_{Cu+Cu}}}{< N_{coll} > \frac{n_{p+p}}{norm_{p+p}}}. \tag{4.6}$$

The transverse momentum distribution of the normalized R_{AA} is shown in Figure 4.4.

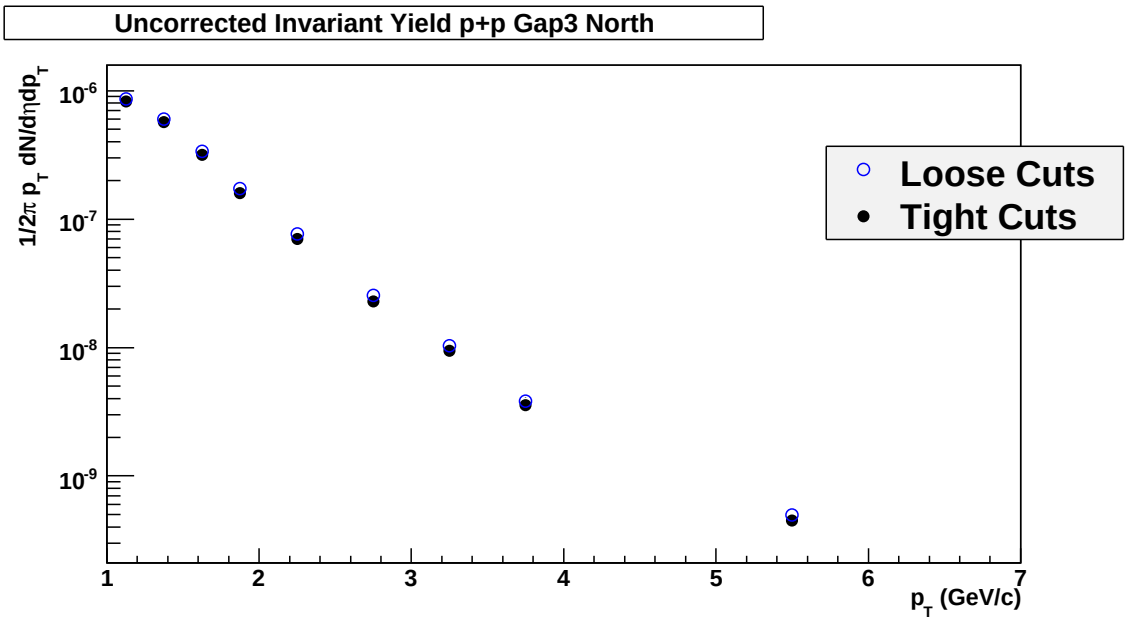

(a)

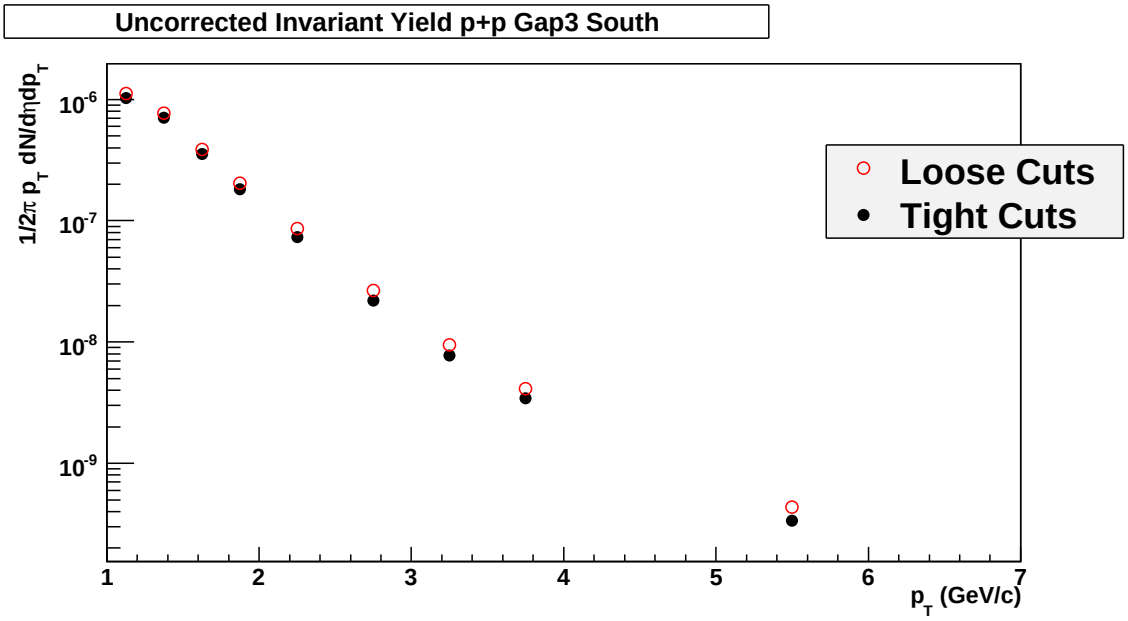

(b)

Figure 4.2: North (blue) and south (red) arm transverse momentum distribution of uncorrected invariant yields for stopped hadrons in Gap 3 produced by $p+p$ collisions surviving all analysis cuts described in Section 4.5. Open circles denote loose cuts and tight cuts are denoted with closed circles.

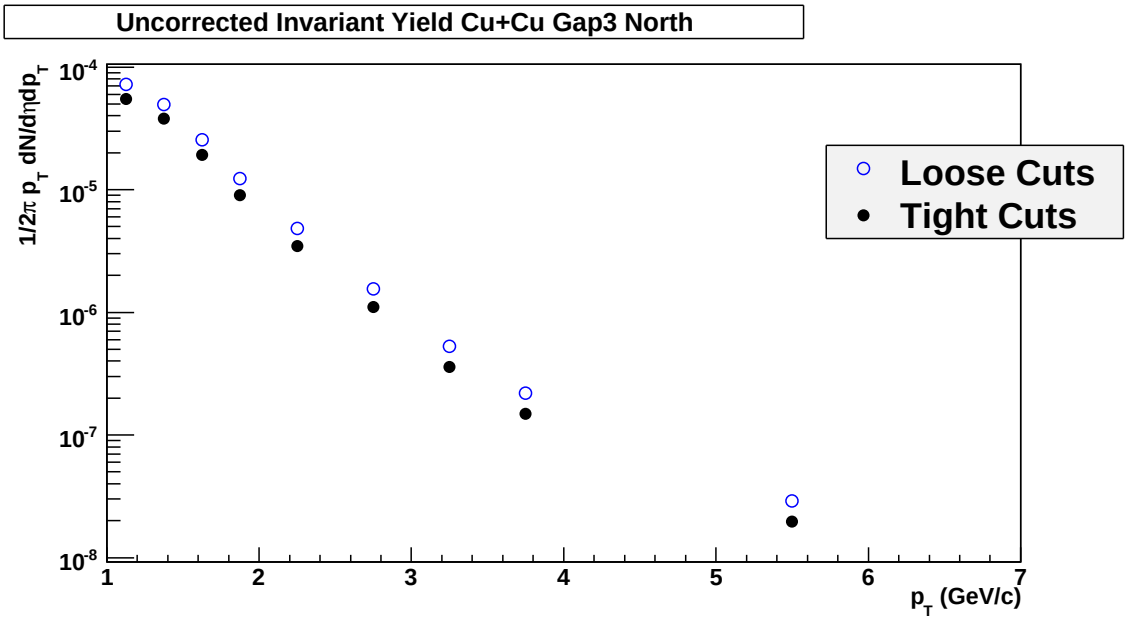

(a)

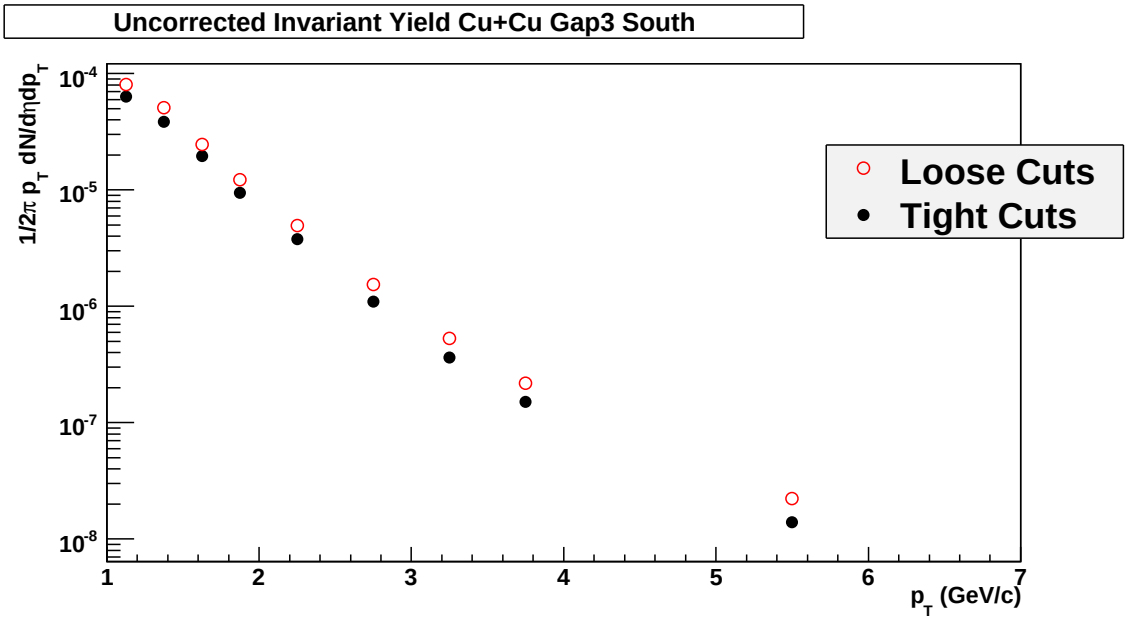

(b)

Figure 4.3: North (blue) and south (red) arm transverse momentum distribution of stopped hadrons in Gap 3 produced by $Cu + Cu$ collisions surviving all analysis cuts described in section 4.5. Open circles denote loose cuts and tight cuts are denoted with closed circles.

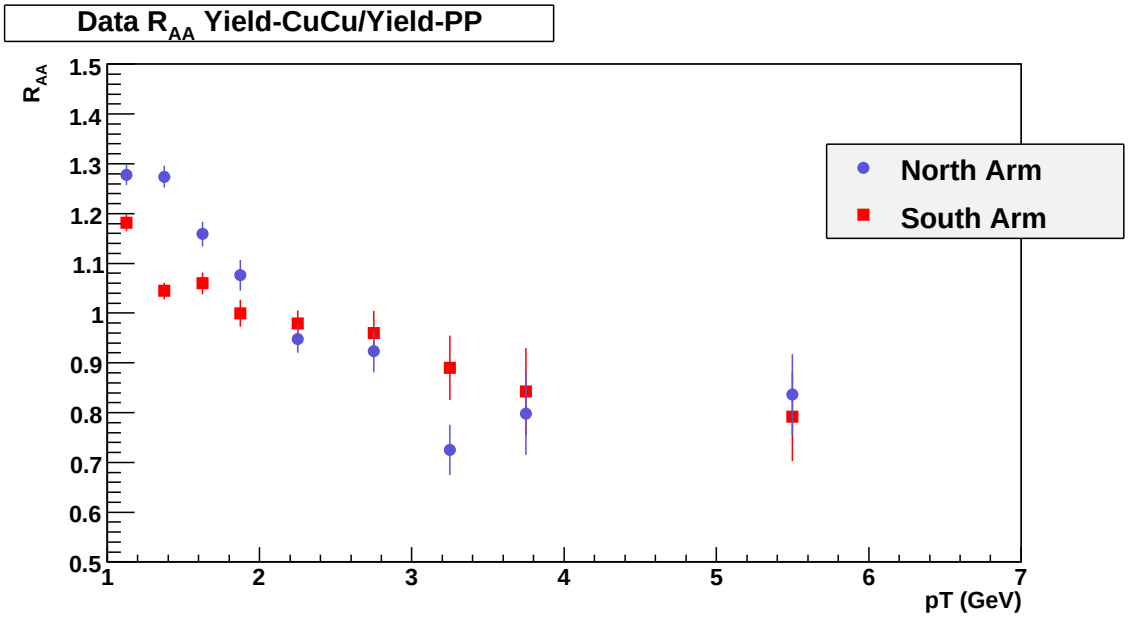

Figure 4.4: Normalized R_{AA} of $Cu + Cu$ and $p + p$ data for stopped hadrons in Gap 3 of the PHENIX detector for the north (blue circles) and south (red squares) arms.

4.4 Simulation Yields

Two hadronic interaction simulation codes are used in this analysis: FLUKA and GHEISHA.

$$\frac{\epsilon_{Cu+Cu}}{\epsilon_{p+p}} \tag{4.7}$$

The ratios of the yields for these packages is shown in Figure 4.5. The differences in these ratios are used to calculate the final R_{AA} result by averaging the two packages together. The average of FL103 and GH93 yields are shown in Figure 4.6. The results shown are used to propagate systematic errors associated with the final R_{AA} result.

4.5 Error Analysis

The two main error types discussed in this analysis are statistical errors and systematic errors (uncertainties). They are uncertainties that are introduced by random fluctuations when taking the measurements and hinder the exactitude of the results in question. We estimate them as well as possible [17].

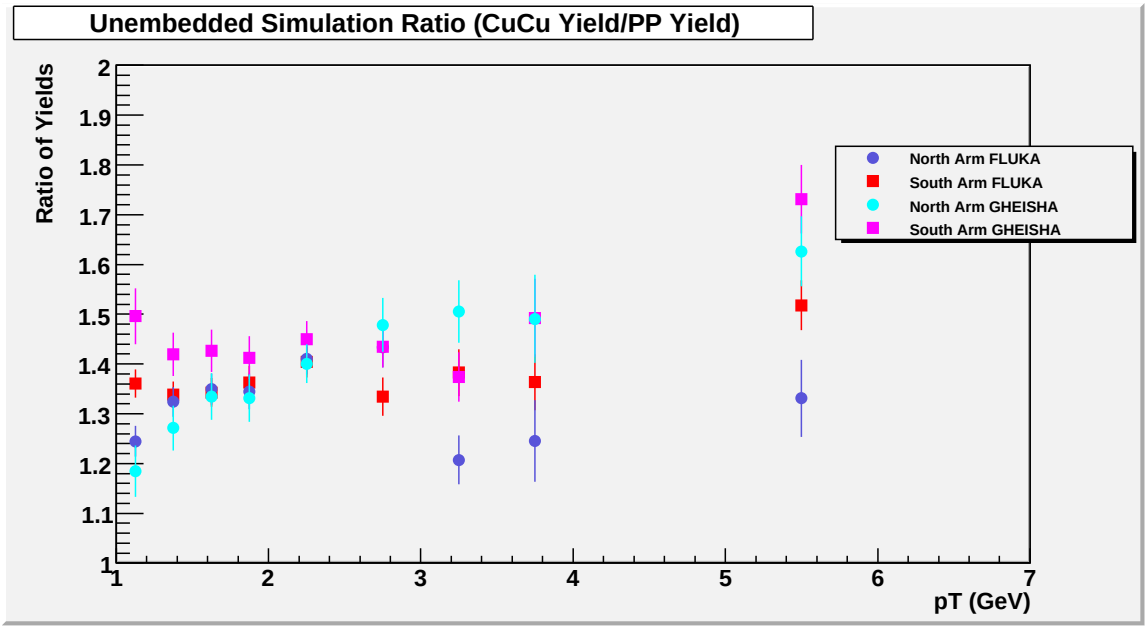

Figure 4.5: Transverse momentum distribution of the ratio of yields for simulation packages FL103 (north and south) and GH93 (north and south).

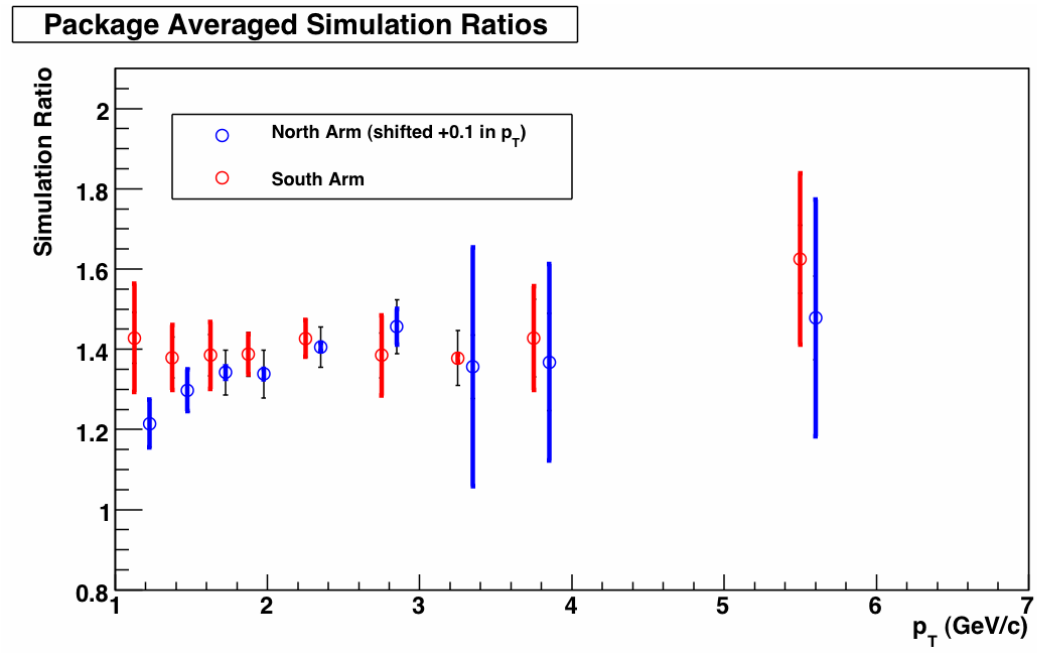

Figure 4.6: Transverse momentum distribution of the ratio of yields for simulation packages FL103 and GH93 averaged (north and south). Systematic errors are represented by bands.

Table 4.1: R_{AA}, statistical errors, and systematic errors for the north and south arms.

Final Analysis Results						
p_T	R_{AA} North	R_{AA} South	Stat. North	Stat. South	Sys. North	Sys. South
1.125	1.278	1.181	0.0602	0.0632772	0.340157	0.345694
1.375	1.274	1.0446	0.0538	0.0508274	0.337242	0.283848
1.625	1.159	1.0598	0.0563	0.0513083	0.301172	0.288824
1.875	1.076	1.000	0.0593	0.0547705	0.27951	0.264222
2.25	0.947	0.979	0.0504	0.0468174	0.246	0.257936
2.75	0.923	0.960	0.0676	0.0560371	0.243	0.266945
3.25	0.725	0.890	0.0795	0.0683953	0.286	0.231086
3.75	0.798	0.842	0.121	0.096423	0.284776	0.244137
5.5	0.836	0.792	0.104585	0.0850466	0.328602	0.266087

In this analysis since there are three measured quantities each with their individual uncertainties, the combination of the information from these measured quantities are used to calculate our final results shown in Table 4.1.

Let A be defined as $A \equiv \frac{N_{Cu+Cu}}{2\pi p_T d\eta dp_T}$ (Figure 4.3) and B (Figure 4.2) be defined as $B \equiv \frac{N_{p+p}}{2\pi p_T d\eta dp_T}$. Also, let C be defined as $C \equiv \frac{\epsilon^{p+p}}{\epsilon^{Cu+Cu}}$.

$$R_{AA} = \frac{A \cdot C}{N_{coll} \cdot B} \tag{4.8}$$

There is also a systematic error associated with N_{coll}. For the multiplication and division of measured quantities, in general, the uncertainties in A and B can be calculated by the following equation.

$$\sigma_{A/B} = \sqrt{\sigma_A^2 + \sigma_B^2} \tag{4.9}$$

And for AC,

$$\sigma_{AC} = \sqrt{\sigma_A^2 + \sigma_C^2} \tag{4.10}$$

The final R_{AA} error propagation can be calculated by adding all error quantities σ_A, σ_B, and σ_C in quadrature and then multiplying by the final result.

$$\sigma_{\frac{AC}{B}} = R_{AA}\sqrt{\sigma_A^2 + \sigma_B^2 + \sigma_C^2} \tag{4.11}$$

Table 4.2: Various sources of systematic error associated with the $Cu+Cu$ yield that need to be accounted for in the analysis.

σ_A		Percent
σ_{A_1}	Gap 3/4 Efficiency Matching, N_H	10%
σ_{A_2}	2^{nd} component, sometimes negligible	1%
σ_{A_3}	$run-to-run$ - A/ϵ	2%
σ_{A_4}	Gap 4 - ϕ differences	5%
$\sigma_{A_{total}}$		11.4%

Table 4.3: Various sources of systematic error associated with the $p+p$ yield that need to be accounted for in the analysis.

σ_B		Percent
σ_{B_1}	Gap 3/4 Efficiency Matching, N_H	10%
σ_{B_2}	2^{nd} component, sometimes negligible	1%
σ_{B_3}	$run-to-run$ - A/ϵ	2%
σ_{B_4}	Gap 4 - ϕ differences	5%
σ_{B_5}	BBC Acceptance	9.6%
σ_{B_5}	Trigger Bias	3%
$\sigma_{B_{total}}$		15.2%

A systematic uncertainty is associated with the Gap 3 stopped hadron yield. Systematic errors and their contributions are shown in Table 4.2, Table 4.3, and Table 4.4. The systematic uncertainties presented in these tables are now discussed.

1. **Gap 3/4 Matching** There is an inherent uncertainty of the MuID tubes and a discrepency in the determination of tube efficiencies. Two methods are used. If the uncertainty of unregistered hit regions in Gap 4 exist, we question how well defined the efficiencies in Gap 3 and Gap 4 are. It affects this analysis 2-fold because Gap

Table 4.4: Various sources of systematic error that need to be accounted for in the simulations.

σ_C		Percent
σ_{C_1}	Gap 3/4 Efficiency Matching, N_H	10%
σ_{C_2}	2^{nd} component, sometimes negligible	1%
σ_{C_3}	$run-to-run$ - A/ϵ	2%
σ_{C_4}	Gap 4 - ϕ differences	5%
$\sigma_{C_{total}}$		11.4%

3 tracks will be higher than they should be for hadrons because they are falsely understood to be Gap 3 due to unregistered hits not firing in Gap 4. In summary, uncertainty exists in the number of tracks going into Gap 3 based on the efficiencies in Gap 4.

2. **2nd component**: This corresponds to the $pd\theta$ distribution and delta z cut to eliminate background. There is uncertainty in the placement of the cut that does not eliminate all background. It is a small issue that has not been completely investigated and does not significantly affect the analysis.

3. **Run-to-run**: For each yearly Run at RHIC there are approximately 600 "runs." There is 1 run/hour taken by the data acquistion system. Fluctuations exist in the behavior of the detector. Some channels go offline as well as trip during operation and must be reset, thus rendering sensitive areas in the detector inconsistent over time.

4. **Trigger Bias**: "The efficiency, or trigger bias of the BBC, ϵ_{BBC} is determined by examining events taken with the non-minimum bias trigger that has tracks. Mid-rapidity pions are used and the BBC is 0.79±0.02 efficient. The BBC trigger bias effect is insignificant for heavy ion collisions due to a larger number of charged particles being produced which increase the overall efficiency of the BBC."

5. **BBC acceptance**: Uncertainty in the BBC for $p + p$ collisions. The BBC is more likely to fire on inelastic collisions. The BBC trigger fires the most often of all triggers at RHIC: it is roughly 23%±2%.

6. **Gap 4 ϕ difference**: The hit patterns of angular distribution of tracks in octants which are possibly (in)active in data but not in simulations. This inactive area is cut, an rms is calculated, and the remaining difference is roughly 5%.

7. **FL103/GH93**: For the same simulation, same cuts, same Run, same MuID tube efficiencies, MuTR efficiencies, identical simulated detector, identical analysis code; this error is obtained by plotting the Gap 3 yield distribution in FLUKA and GHEISHA and calculating that ratio. Anything that deviates from 1 is due to statistical fluc-

tuations or inherent differences in the packages. The width of the distributions of analysis variables in each package is different.

8. **Cocktail Input**: Uncertainty exists because we do not have true measured hadron distributions for the 1.4 to 2.0 rapidity window at RHIC. There are only available at y = 0 and at y = 3.0, so an estimate must be made.

9. **MuID**: Since the MuID gaps include two sensitive layers, about 18% of the North Arm Gap 4 is susceptible to trigger ineffieciency of this magnitude.

It is possible to combine the north and south arm measurements by averaging the central values. Care must be taken to successfully total the systematic uncertainties. The sum of combined arm systematic uncertainties is $\sigma_{\frac{North+South}{2}}$ and is calculated by factoring in the correlated and uncorrelated uncertainties.

The correlated errors are essentially the same for both arms. While the values are actually different at some level because of different signal to background ratios which then result in numerically different uncertainty values, it is acceptable to average the two correlated errors which allows for a straightforward uncertainty propagation calculation given by a previous equation. The point-to-point uncorrelated uncertainties remain amalgamated with the statistical uncertainty bars, as was performed for individual muon arm measurements. The systematic uncertainty associated with the acceptance and efficiency corrections is the four components given in the table added in quadrature. For the uncertainty in this analysis and potentially others, the same values are used for both the north and south muon arms. The final calculations for the analysis can be found in Table 4.1 and the final R_{AA} result plot including systematic and statistical errors is shown in Figure 4.1.

Place holder.

4.6 Hadron Identification in the PHENIX Muon Arms

Unidentified hadrons are measured using particles that stop in the MuID shallow gaps. There are 5 gaps in the PHENIX MuID detector, numbered 0 through 4. After a collision occurs, the resulting particles are detected by plastic proportional tubes called Iarocci tubes in each gap. There are layers of steel separating layers of Iarocci tubes (as depicted

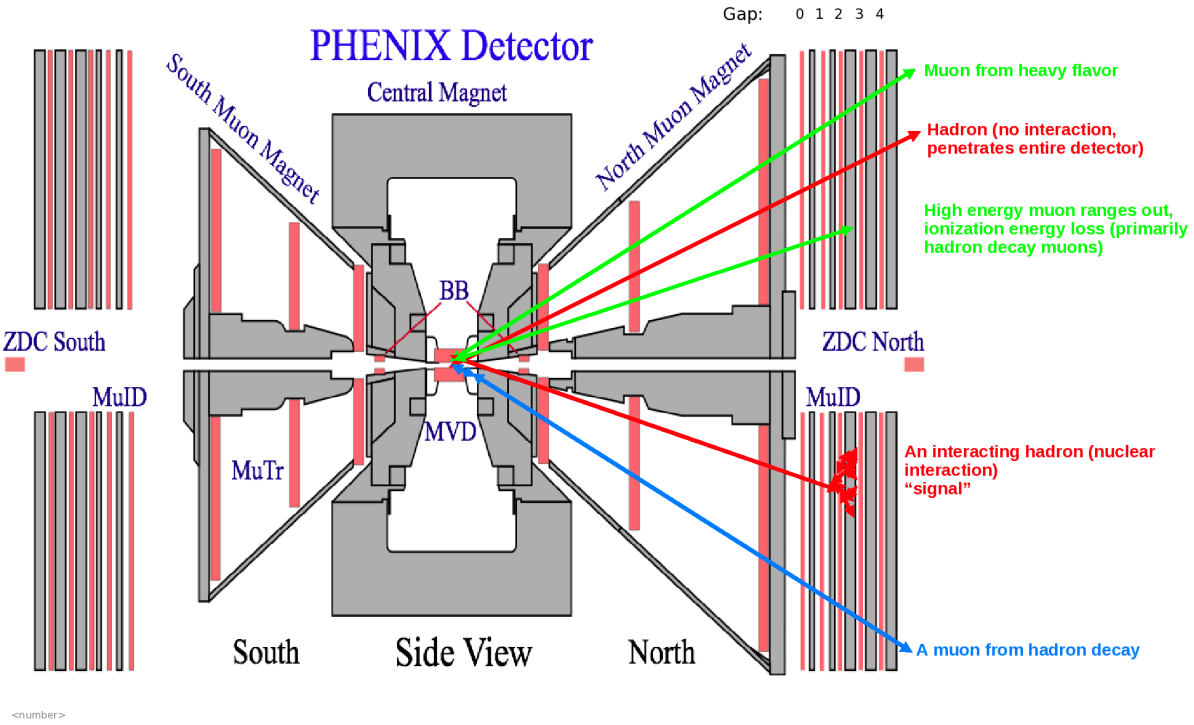

Figure 4.7: Path of some possible tracks in PHENIX.
1)High energy muon that penetrates the entire detector.
2)Hadrons that do not interact with the steel and penetrate through the entire detector. These are usually referred to as "punch through."
3)Low energy muons that "range" out due to ionization energy loss. These are primarily decay muons.
4)Hadrons may experience nuclear interaction with the steel shielding in the detector and stop in a shallow gap. These stopped hadrons are the signal used for the analysis presented in this thesis.
5)Muons from hadron decay penetrate the entire detector. These are referred to as "decay muons." These "decay muons" are background for this analysis.

in Figure 2.4) followed by gaps (of active detector volumes) that measure the position of the particles. The steel provides the hadron rejection factor which permits separation of hadrons and muons. When particles pass through an active detector volume, a "hit" is recorded. The trajectories of these different particles are called "tracks." A track is formed from a collection of hits in the detector. The collisions produce thousands of hits in total that are recorded by the detector's electronics. A classification scheme of the types of tracks is shown in Figure 4.7.

Figure 4.7 shows different possible track paths in the muon arm. 1) The low energy decay muons that "range out" due to ionization energy loss can register hits in Gap 2, 3, or 4. 2) Even with the great probability the hadrons have of interacting with the steel, some small percentage of the total hadrons will get through the 1.5 m of steel and end up being detected in the final gap of the MuID which is Gap 4. This portion of the hadron population is estimated by Monte Carlo simulations (hadron cocktail) because PHENIX is not capable of separating these experimentally from muons. 3) High energy muons that pass through the entire detector, such as for measuring J/ψ. They primarily stop in Gap 4 but a small number stop in Gap 3. 4) Hadrons experiencing the nuclear interaction with the steel in the detector may stop in Gap 2, 3, or 4. Muons from light hadron decays will penetrate the steel absorber layers in the detector.

There are three main interactions responsible for energy loss in particles traveling through the detector. They are multiple scattering (electronic ionization), due to electrons in the outer shell of the atoms in the steel, electronic ionization due to the protons in the nucleus of the atom, and the strong interaction.

The mean energy loss per unit thickness $\frac{dE}{dx}$ can be used to calculate how deep a particle will most likely penetrate and pass through the detector material. Since different detectors use different materials depending on their physics goals, the density of material used in the detector is important. So, based on the particle's momentum and energy, the choice of material will be determined using the knowledge that there is a proportional relationship between energy of particle and distance traveled through the medium. In the case of the PHENIX experiment, steel is used to separate background from signal. [18]

Muon candidates with sufficiently high momentum penetrate to the deepest sensitive layer in the MuID Gap 4 which is 8.7 m from the interaction point (IP), or collision vertex.

The total thickness of steel between the event collision vertex and the deepest layers of the MuID is 1.50 m. Hadron susceptability in material can be calculated to some approximation by $e^{\frac{-L}{\lambda_I}}$, where L is the total depth of absorber material and λ_I is the nuclear interaction length at a specific momentum for a specific hadron in a particular material. For this analysis, it is advantageous to assume the hadron is a pion of momentum-averaged λ_I of about 0.16 m of steel. By putting these assumptions to use, one can calculate that the 9.5 λ_I of steel in the muon arms provides a total hadron rejection of $e^{-9.5}$, on 1/10000.

When observing particles stopping in a gap other than the last gap, it is possible to have hadrons or muons that range out. As shown in Figure 4.8, the ranged out muons are confined to a relatively narrow band in longitudinal momentum. The width of the peak, σ, is set by mostly the thickness of steel in between Gap 3 and Gap 4. The minimum p_z is determined by the total amount of steel up to Gap 3. Then the particles below a p_z of 2.7 GeV/c can not make it to the last gap. So, by not observing tracks in Gap 4, an approximate 2σ standard deviation cut, used to calculate the placement at 2.7 GeV/c cut indicated by the vertical red line shown in Figure 4.8, eliminates the majority of background within the analysis. Therefore, we can rather cleanly identify hadrons above a p_z of 2.7 GeV/c [19].

4.7 Definition of Analysis Variables

The systematic cuts used in the analysis are defined in this section [9]. Cut values were obtained by fitting the particular cut value's histogram with a guassian function. A 3σ cut is then made to eliminate virtually all background attributed to the particles not satisfying this condition.

1. BBC z-vertex - z vertex of the event collision as determined by the BBC detector discussed previously in Section 2.4. This analysis considers particle tracks within the range of -30 cm $\leq z \leq$ 30 cm, the free flight path range of hadrons which is a subset of all particles coming from the wide vertex distribution of the collision measured by the BBC.

2. Number of MuTR hits - As described in Section 2.5, the MuTR has three stations

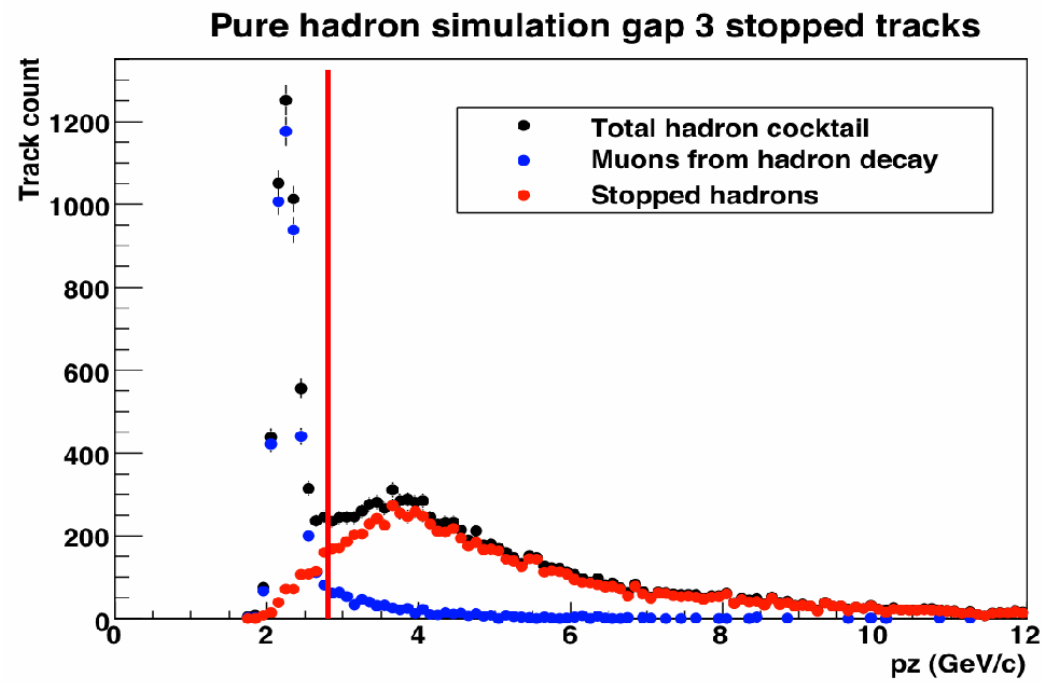

Figure 4.8: Longitudinal momentum distribution of track count for simulated single hadrons stopping in Gap 3.

per arm and can have up to 16 hits per track. A maximum of six hits each in Stations 1 and 2 can be recorded, while Station 3 can have a maximum of four hits.

3. RefRad - This variable is the extrapolated radial offset of the track corresponding to the MuID road at z=0. The value is computed from the different Δx and Δy offsets at z=0 using $\Delta x^2 + \Delta y^2$ as shown in Figure 4.9. The offsets are retrieved by extrapolating to z=0 the one-dimensional rate of change in either x or y of the MuID road through the Gap 0 hit coordinate. Distributions are shown in Figures 4.10(a) and 4.10(b).

4. Road Slope - Slope of the MuID road determined from the 2D-road. A minimum slope is taken to ensure the MuID square hole is avoided.

5. DG0 - Distance at Gap 0, is the difference between the MuTR track projection and the MuID road projection at MuID Gap 0. The units of DG0 are in centimeters. Distributions are shown in Figures 4.12(a) and 4.12(b).

6. DDG0 - is the angle between the MuTR track projected and the MuID road projection

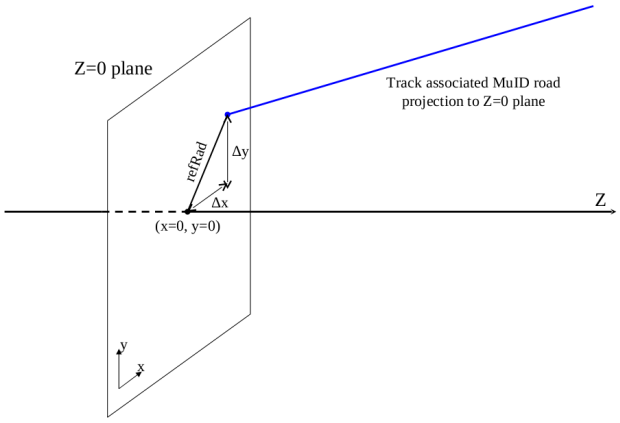

Figure 4.9: Definition of analysis cut variable refrad.

at MuID Gap 0. The units of DDG0 are degrees and are shown in Figure 4.13(a) and Figure 4.13(b).

7. p$\delta\theta$ - measures the extent of deflection due to multiple scattering that a track undergoes in the pre-MuTR absorber. The product of a particles multiple scattering angle and a momentum remains approximately constant for all momenta. Figure 4.14 indicates this deflection measurement schematically.
8. δz - is the difference between the event vertex as determined by the BBC, with a 2 cm resolution for $p+p$ and 0.5 cm for $Cu+Cu$ and the vertex determined by the muon track-refit algorithm in the muon tracking software.

Along with these kinematic cuts, other parameters in the analysis should also be mentioned for $Cu+Cu$ and $p+p$, respectively. For minimum bias events, the magnetic field used in the $Cu+Cu$ collisions for Run 5 was set to B.

ROOT "TCuts" were applied "to miminimize the effect of the run to run variation in the detector acceptance in the data that is hard in practice to accomplish in simulations, seperate standard geometric acceptance cuts are placed on both the data and simulations. This allows for the maximization of agreement between data and simulation, even if simu-

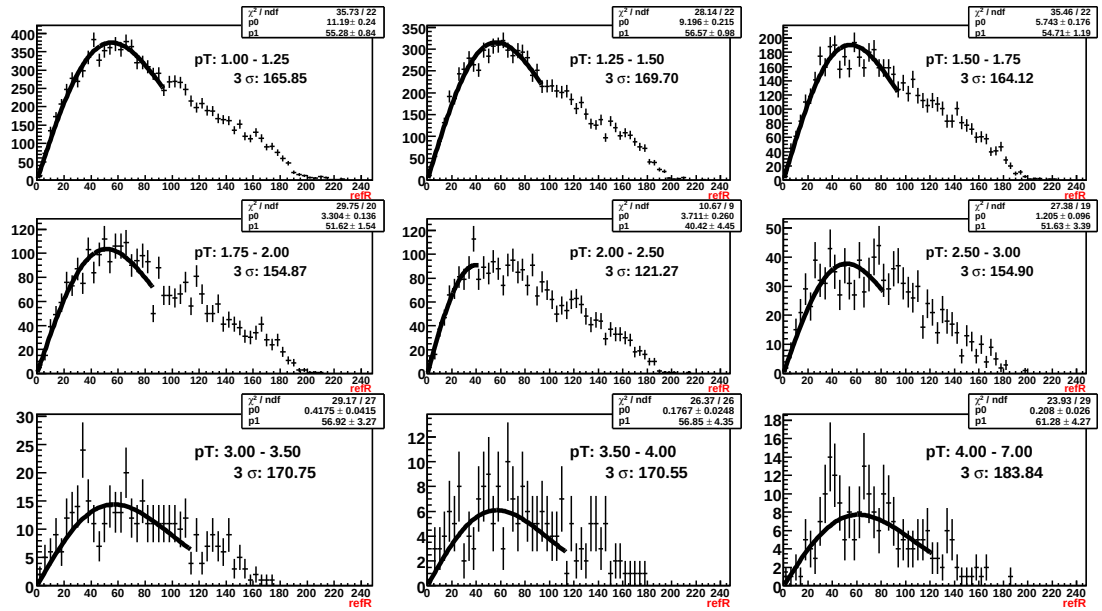

(a) RefRad South Arm plot.

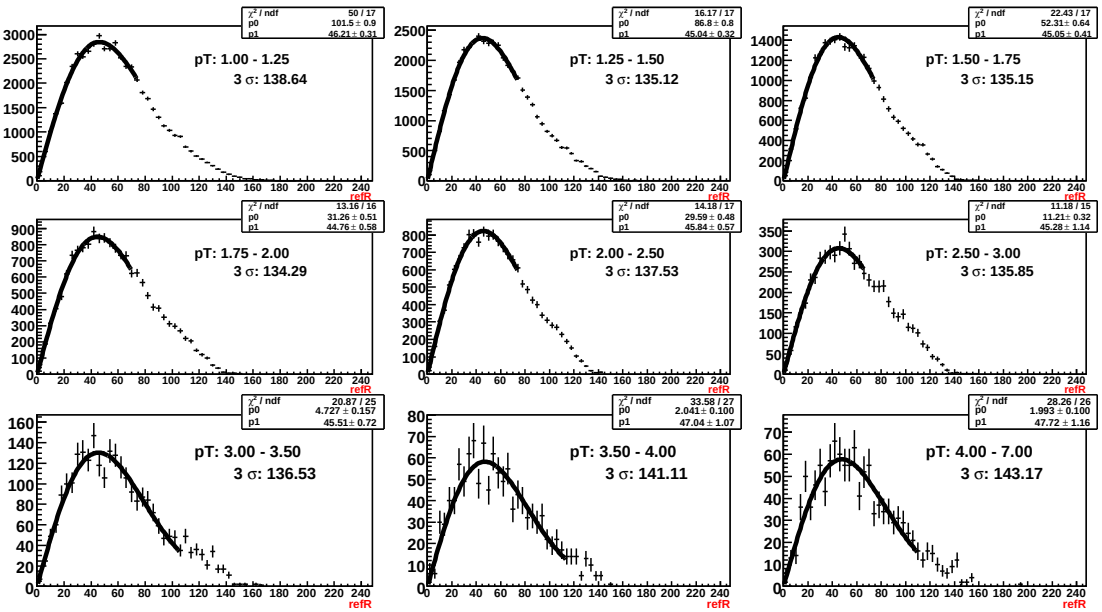

(b) RefRad North Arm plot.

Figure 4.10: South and north RefRad distributions with 3σ standard deviation cut values shown by solid lines.

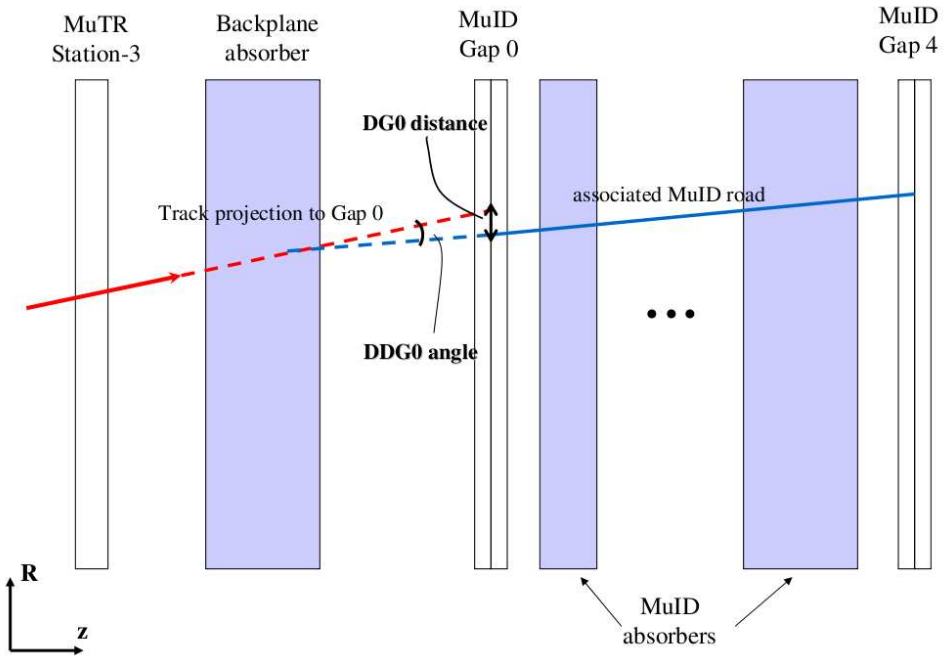

Figure 4.11: Definition of analysis cut variables DG0 and DDG0.

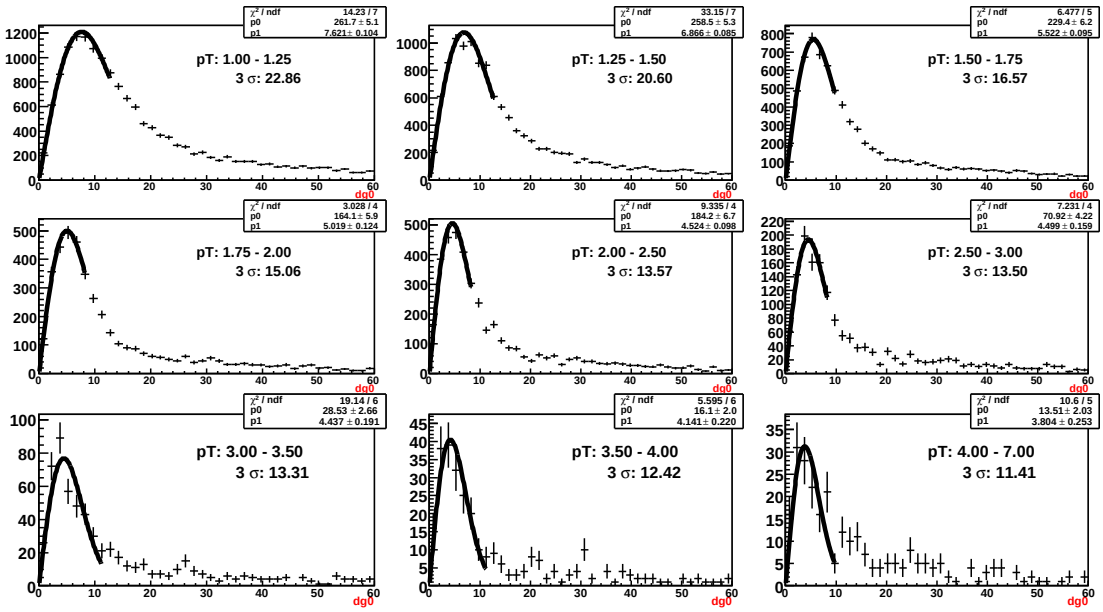

(a) DG0 South Arm plot.

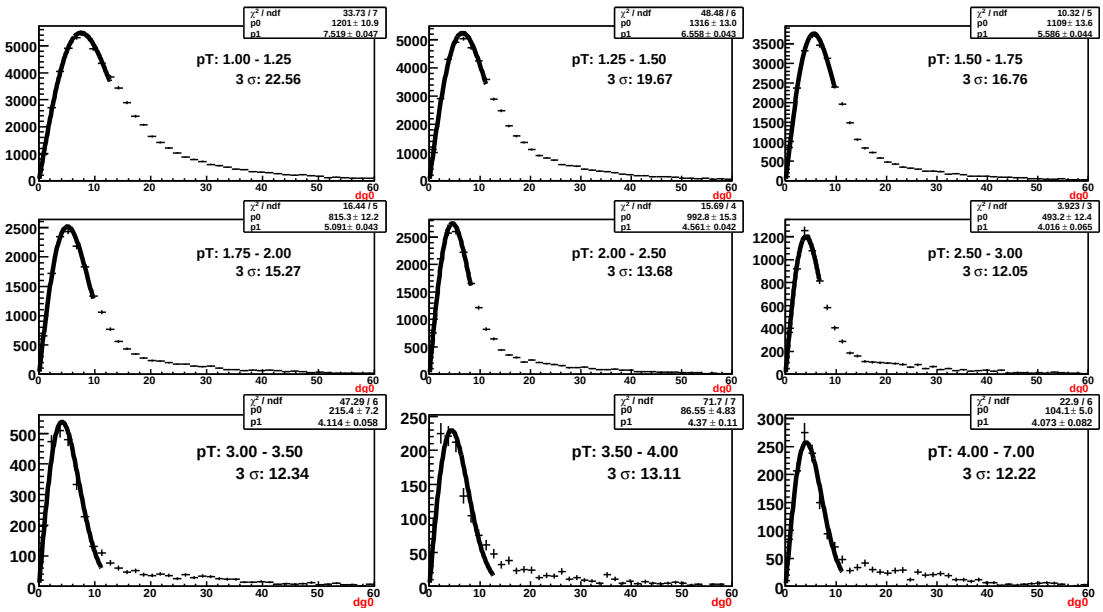

(b) DG0 North Arm plot.

Figure 4.12: South and north arm DG0 distributions with 3σ standard deviation cut values shown by solid lines.

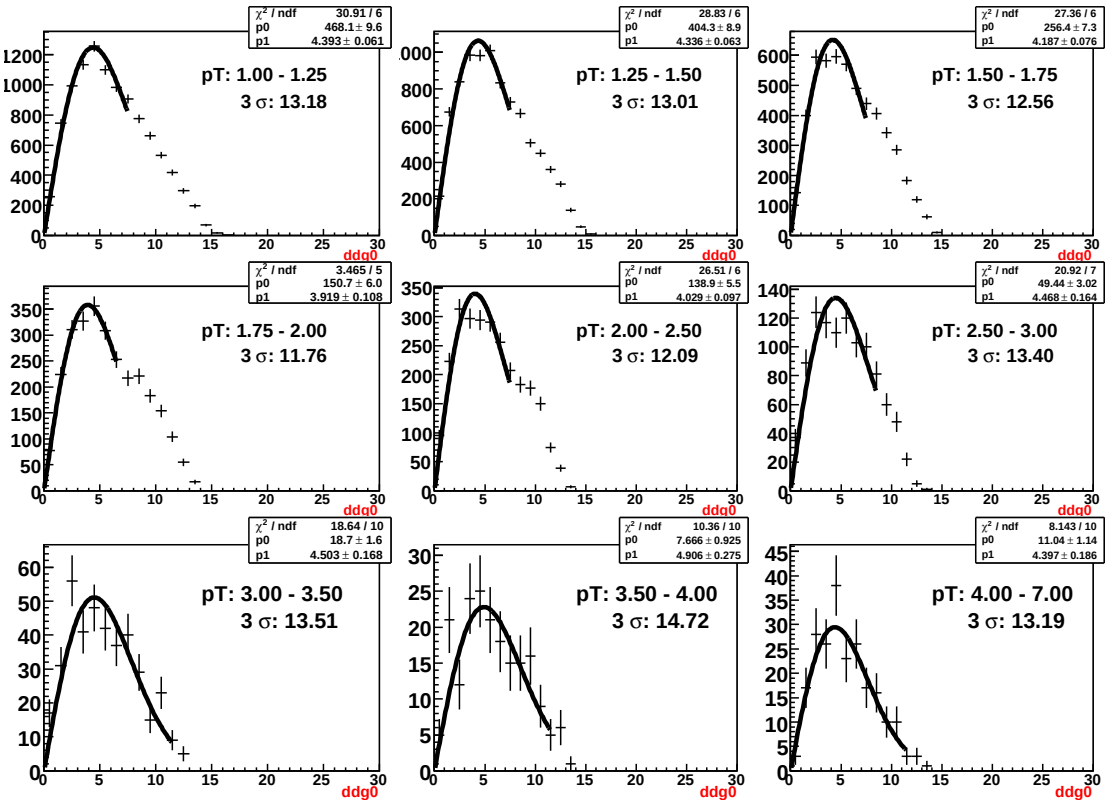

(a) DDG0 South Arm plot.

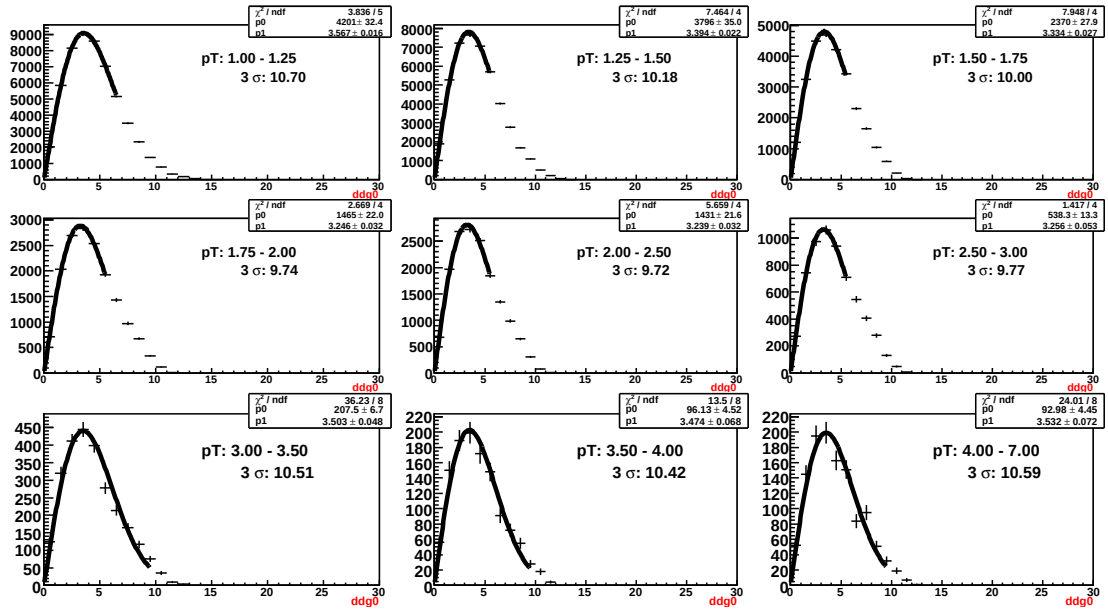

(b) DDG0 North Arm plot.

Figure 4.13: South and north arm DDG0 distributions with 3σ standard deviation cut values shown by solid lines.

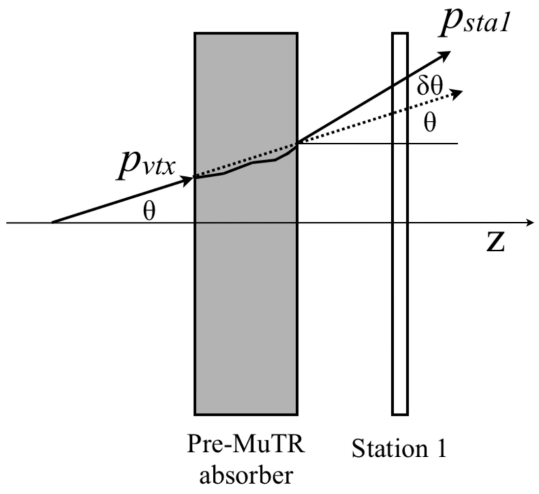

Figure 4.14: Definition of analysis cut p$\delta\theta$ [9].

lation uses very few run numbers to specify the detector response function." [6]

There were ϕ cuts that were also applied. "The ϕ and radial hit distributions are compared using the hadron cocktail by examining all three MuTR stations and Gaps 2, 3, and 4 of the MuID. Acceptance is restricted to specific radial and phi regions for both simulations and data to maximize agreement in the tracks accepted for the analysis. The root mean square (rms) of the ratio of the simulation/data for these distributions form one of the components used in the determination of the systematic uncertainty in the Acceptance $\times$ Efficience correction (Aϵ)." [6]

For $p+p$ collisions, the 1D trigger emulator and 1S trigger emulator along with ϕ cuts and TCuts were all implemented [6].

It was determined that two trigger fibers were swapped incorrectly in the Run 5 $p+p$ analysis, altering the data acquired. The trigger emulator accounts for this in the analysis.

4.8 Application of the Analysis Cuts

Analysis cuts are imposed on a track-by-track basis. The track selection criteria for the accepted pseudorapidity interval $1.4 \leq \mid \eta \mid \leq 2.0$ is discussed below. In general 3σ cuts are used to eliminate a significant amount of background from the statistics. The values of these cuts are provided in Table 4.5 and Table 4.6.

Table 4.5: Analysis cuts for the variables DG0 and DDG0.

		$Cu+Cu$		$p+p$	
	p_T	North	South	North	South
$DG0(^\circ)$	0	15.26	24.88	14.75	28.59
	1	15.19	20.39	14.05	26.03
	2	14.45	18.10	13.45	22.63
	3	13.41	15.52	13.05	19.84
	4	13.15	14.66	12.42	16.95
	5	13.00	13.00	12.38	14.36
	6	13.00	12.52	14.25	14.47
	7	13.00	12.52	14.71	13.69
	8	13.00	12.52	14.49	12.84
DDG0 (cm)	0	13.14	14.64	11.78	11.78
	1	12.84	14.34	10.87	10.87
	2	12.67	14.14	9.82	9.82
	3	12.55	13.96	9.43	9.43
	4	12.52	13.23	9.17	9.17
	5	12.50	12.44	9.27	9.27
	6	12.50	12.00	10.70	10.70
	7	12.50	12.00	10.86	10.86
	8	12.50	12.00	10.89	10.89

Table 4.6: Analysis cuts for variables δz and vtx.

		$Cu+Cu$		$p+p$	
	p_T	North	South	North	South
δz (cm)	0	-2,2	-2,2	-2,2	-2,2
	1	-2,2	-2,2	-2,2	-2,2
	2	-2,2	-2,2	-2,2	-2,2
	3	-2,2	-2,2	-2,2	-2,2
	4	-2,2	-2,2	-2,2	-2,2
	5	-2,2	-2,2	-2,2	-2,2
	6	-2,2	-2,2	-2,2	-2,2
	7	-2,2	-2,2	-2,2	-2,2
	8	-2,2	-2,2	-2,2	-2,2
vtx (cm)	0	161.07	170.78	170.78	161.07
	1	150.04	177.74	177.74	150.04
	2	137.84	165.24	165.24	137.84
	3	135.78	156.36	156.36	135.78
	4	133.84	139.31	139.31	133.84
	5	138.26	154.23	154.23	138.26
	6	150.24	187.16	187.16	150.24
	7	150.58	173.65	173.65	150.58
	8	154.65	179.65	179.65	154.65

For this analysis the term "loose" cuts will be designated as all tracks involved in the collision: this means no analysis specific cuts are applied. On the contrary, the term "tight" cuts will be designated to mean all acceptable tracks that meet all the selection criteria for the analysis. A factor of approximately 30% decrease in tracks can be seen at high p_T which we attribute to the "tight" cuts applied in the analysis. Invariant yield for $p+p$ data with "loose" and "tight" cuts are displayed in Figure 4.2 and Figure 4.3. The $Cu+Cu$ yields are for the north and south arms displayed in Figure 4.3(a) and Figure 4.3(b), respectivelys. From this factor, it can be inferred that more background is removed from the data observed in $Cu+Cu$ collisions as expected due to the larger particle multiplicity in $Cu+Cu$ collisions relative to $p+p$.

4.9 Simulations

Simulations in the analysis estimate the relative efficiency and observe its dependence on the hadronic interaction package. Efficiency is the likelihood of reconstructing a given particle while acceptance is defined as active area of the detector. The simulation results are folded into the final R_{AA} result as shown in Eq. 4.3. The differences in the simulation codThere is also a systematic error associated with N_{coll}.es largely cancel for a relative efficiency calculation. Simulations quantify the degree to which the relative efficiency and assumption of independence of the simulation packages agree or disagree.

The hadron cocktail is a prescription for the relative yield abundance of particle species ratio as a function of p_T. The primordial mix of pions and kaons is processed through GEANT and the muon arm response-reconstruction software chain. The K/π simulation ratio is derived from PHENIX central arm K/π measurements. The acceptance and efficiency cuts used are documented in a colleague's thesis [9].

A version of the hadron cocktail is produced consisting of a particular hadron shower code and a scale value for the steel hadron interaction cross section [9]. Uncertainty in the quantitative description of hadronic interactions in the two different hadronic packages, FLUKA and GHEISHA, lends to different values for their corresponding absolute acceptance and efficiency. It differs by a factor of 2. Fortunately, it is not necessary to measure the absolute acceptance, all that is needed is the relative acceptance and efficiency. Using the two different hadron interaction packages assess the systematic error with the fact that it is a complete unknown. The ratios of the yields for these packages is shown in Figure 4.5.

In Figure 5.1 the nuclear modification factors for simulation packages FLUKA and GHEISHA are averaged together for minimum-bias $Cu+Cu$ and $p+p$ collisions at $\sqrt{s_{NN}}$ = 200 GeV at forward rapidity and separated by north(blue) and south(red) arms respectively. This result is obtained by simply dividing uncorrected invariant simulation yields N^{Cu+Cu} by N^{p+p} and multiplying the number of binary collisions $N_{coll} = 52.3$ as shown in Equation 4.2. Error bars represent the statistical errors. The shaded bands represent the systematic errors associated with the differences in simulation codes FLUKA and GHEISHA of these quantities without other contributions.

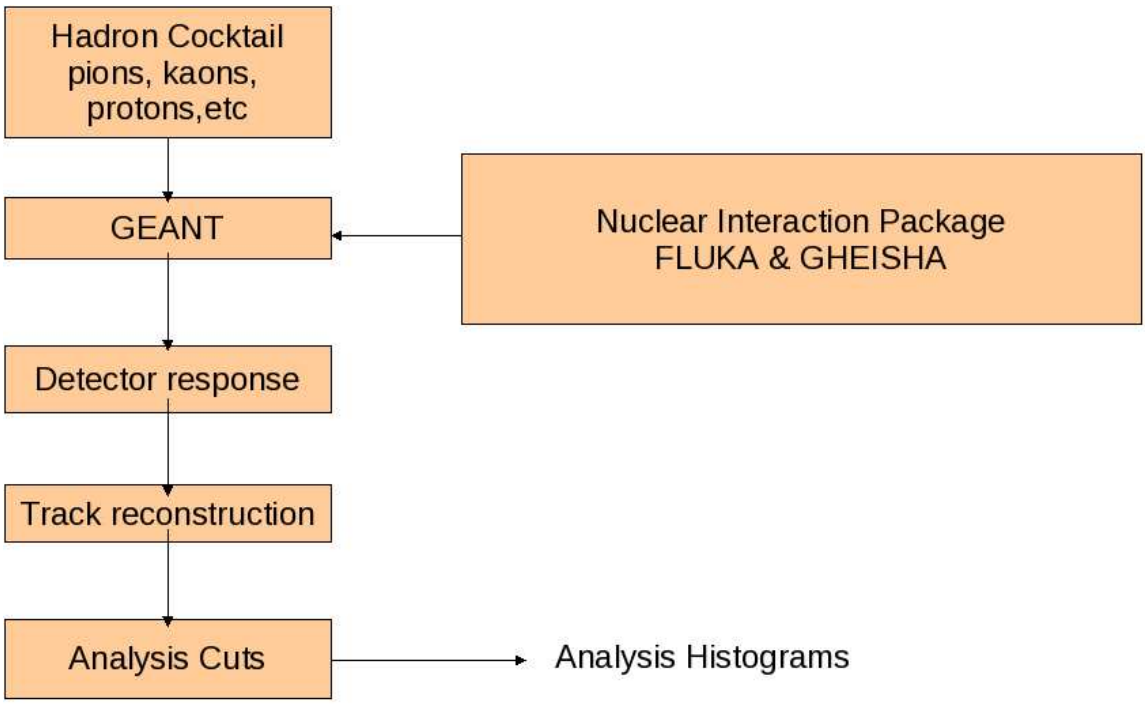

Figure 4.15: Flow chart for hadron cocktail simulations.

Chapter 5

Results

5.1 Overview

This chapter addresses the final results of this thesis. The results of other physicists within the PHENIX collaboration are presented in chapter 6 for a comparison. As described previously, in the absence of modifications due to initial-state or final-state effects, the rate of production of particles through hard processes in nucleus-nucleus collisions is expected to decrease with respect to the given equivalent $p + p$ hard binary collisions scaled by N_{coll} [6].

The primary physics result from this research, R_{AA}, is calculated using measured p_T spectra. This investigates "hot" nuclear matter and confronts some issues in the overall RHIC QGP study of nuclear matter effects. This research has produced a coherent framework for PHENIX to make the first ever R_{AA} measurement of a purified sample of stopped hadrons at forward rapidity using $Cu + Cu$ collisions at $\sqrt{s_{NN}} = 200$ GeV with $p + p$ collisions as a baseline using the stopped hadron measuring method.

The R_{AA} of $Cu + Cu$ is shown in Figure 5.1. Figure 5.1 shows a suppression of hadron production for all transverse momenta. The suppression increases with transverse momentum up to 2.0 GeV/c and seems to saturate at higher momentum. The strong hadron suppression at forward rapidity suggests that the hot, dense, partonic medium may also exist in the forward rapidity region. These observations are consistent with a model where a dense strongly interacting partonic matter with strong collective flow is most likely formed

in minimum bias collisions over a rapidity range of 1.4 to 2.0 which results in strong suppression of charged hadron yields. The data from the north and south arms disagree with a statistical and systematic uncertainty below a p_T of 1.0 GeV/c and agrees for p_T greater than 2.0 GeV/c. The results are consistent with what is observed at mid-rapidity and generally interpreted in terms of energy loss of the partons that fragment into the observed hadrons.

In Figure 5.2, R_{AA} of $Cu + Cu$ for unidentified hadrons with north and south arms averaged at forward rapidity decreases from 0.95 to 0.57 with increasing p_T from 1.0 GeV/c to 5.5 GeV/c indicating that hadron yields are suppressed with respect to $p + p$ collisions. Moreover, the hadron yields allow for the possibility that nuclear effects other than parton energy loss, or jet quenching, may be responsible for the strong suppression. Other nuclear effects that might be contributing to the suppression include gluon saturation and a new hadronization mechanism other than parton fragmentation. One possible source of uncertainty in the high-p_T suppression is inelastic scattering of hadrons after fragmentation [6]. Note that for p_T less than 2.0 GeV/c, the R_{AA} is less than 1.0. At low transverse momentum there are soft processes at work that can effect R_{AA}.

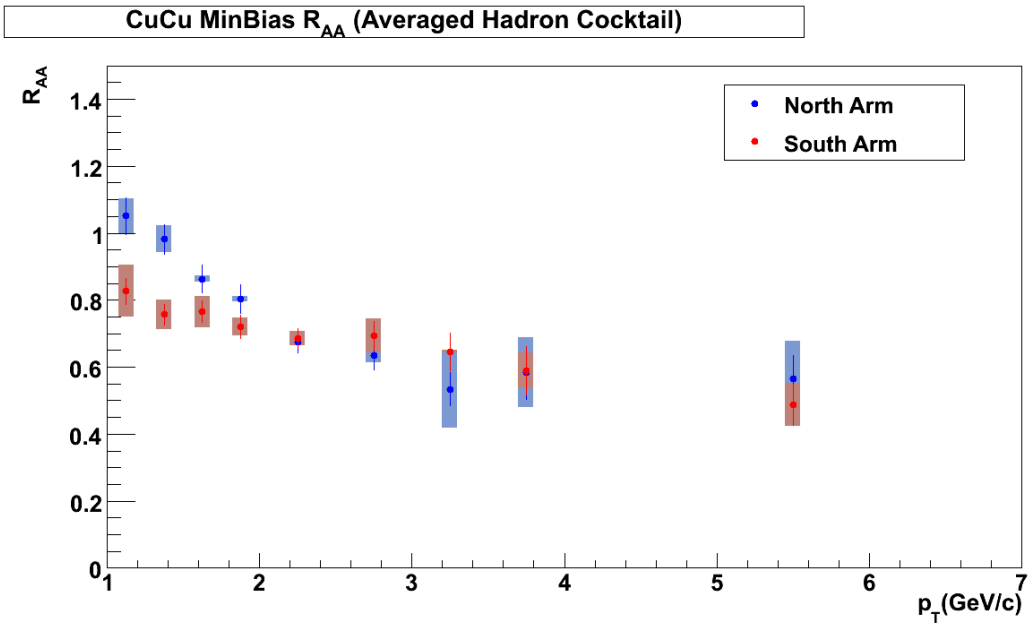

Figure 5.1: Transverse momentum distribution of R_{AA} for stopped hadrons in Gap 3 of the MuID for north (blue) and south (red) arms. Statistical errors (vertical lines) are propagated when dividing histograms.

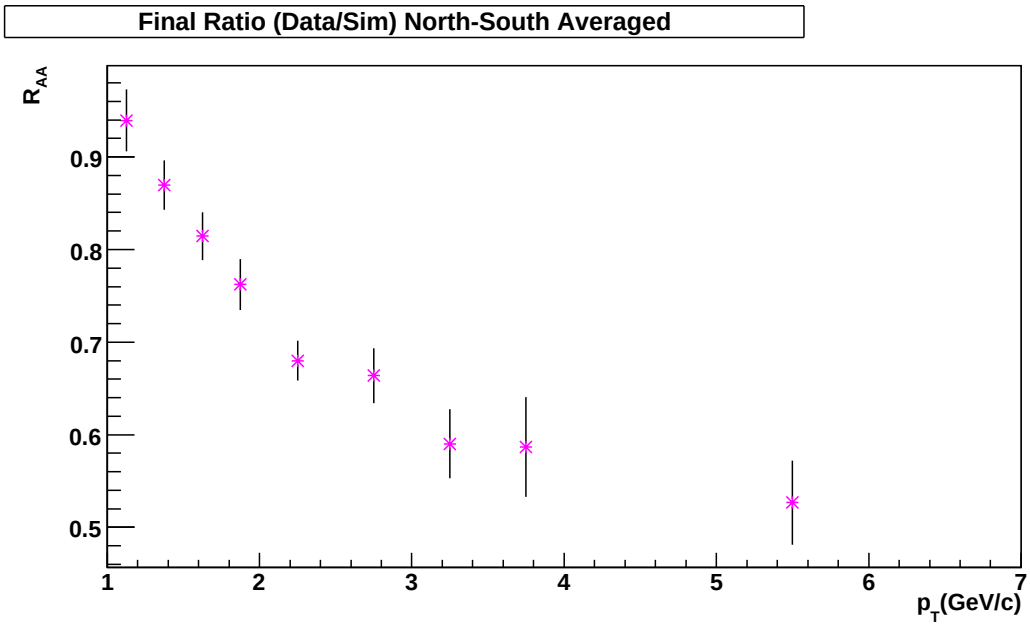

Figure 5.2: Transverse momentum distribution of R_{AA} for stopped hadrons in Gap 3 of the MuID for minimum bias $Cu + Cu$ collisions at $\sqrt{s_{NN}} = 200$ GeV at forward rapidity. The north and south arms averaged. The R_{AA} value is decreasing as p_T increases.

Chapter 6

Discussion

The R_{AA} analysis presented in this thesis falls into the category of measurements not originally foreseen in the planning stages of the PHENIX detector. The measurement of R_{AA} of stopped hadrons in a detector not optimized for this observation creates opportunities for further topics of study in heavy-ion physics. Before pursuing PHENIX publication, additional work must be done to at least reach PHENIX Preliminary status extending the analysis with centrality binning. This chapter will discuss results, a to-do list for future work, and the possibility of using this method in other codes.

The general hypothesis is that the nucleus of an atom is an independent superposition of protons and neutrons. One would naively expect that there would be no nuclear effects therefore R_{AA}=1.0. Measurements of R_{AA} and quantification of deviations of R_{AA} from 1.0 in hot and cold nuclear matter for hadron production provide further insight into the nuclear environment and the magnitude of the nuclear effects at RHIC. Previous R_{AA} results at RHIC are shown in Figure 6.1.

6.1 Comparison

Figure 6.2 shows that the R_{AA} for unidentified hadrons measured in this analysis at forward rapidity agrees with the R_{AA} measured at y=0 by PHENIX for identified π^0s in minimum bias $Cu + Cu$ collisions. The other symbols display measurements from the PHENIX central arms compared to several centrality bins [20].

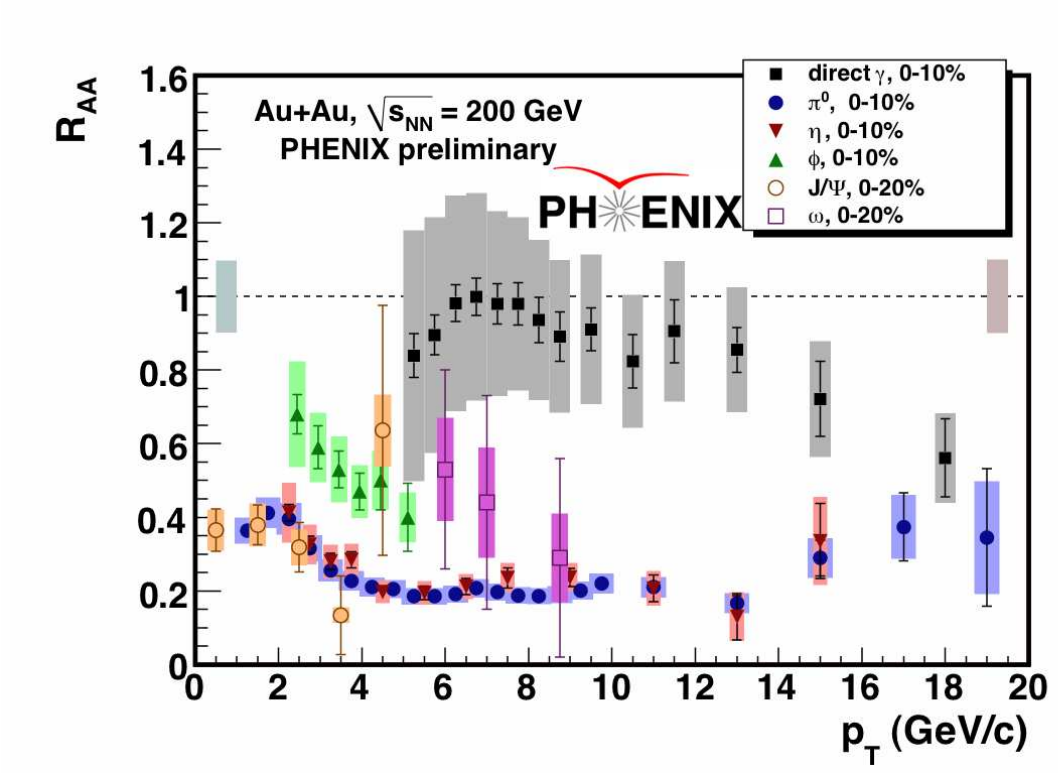

Figure 6.1: Previous PHENIX measurements of R_{AA} with slightly different centralities for $Au + Au$ collisions for species η, γ, ω, J/ψ, and π^0 at y=0.

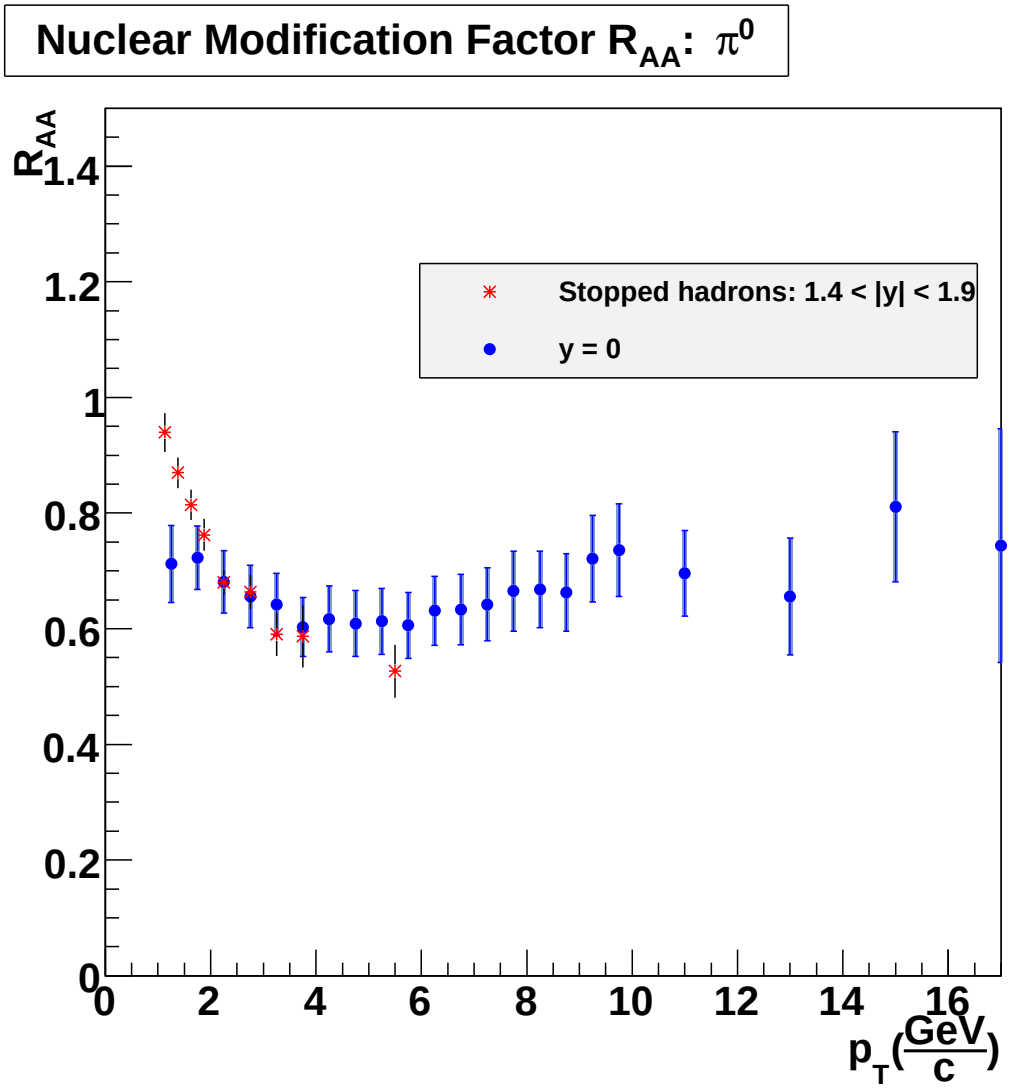

Figure 6.2: PHENIX transverse momentum distribution of R_{AA} $Cu + Cu$ collisions: minimum bias π^0s (blue) at y=0 and minimum bias stopped hadrons (red) result at $1.4 \leq$ y ≤ 2.0.

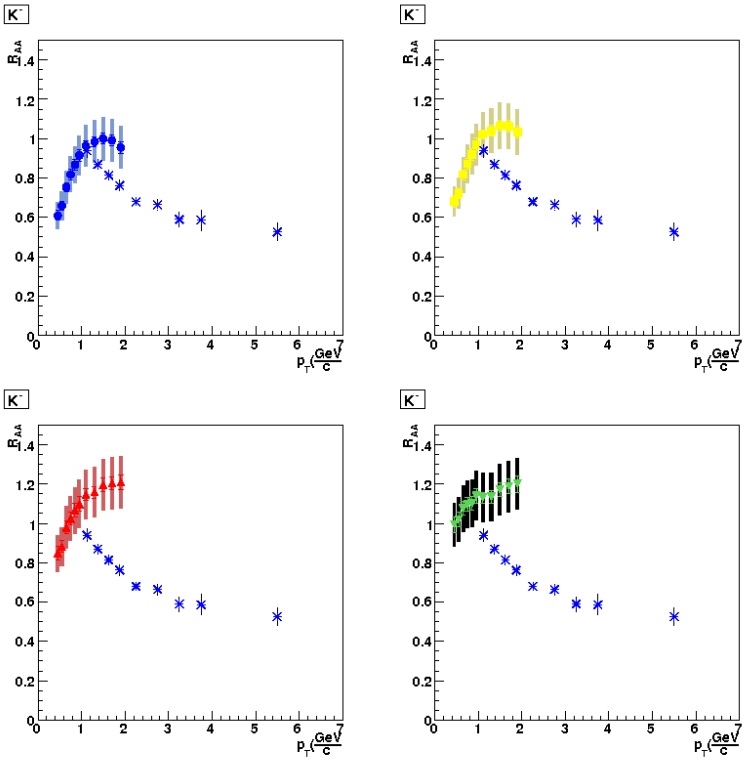

Figure 6.3: Transverse momentum distribution of R_{AA} for the analysis (blue asterisks) compared to K^- particles [20]. The upper left graph displays R_{AA} for centrality 0-10%. The graph to the right of the upper left graph shows R_{AA} for centrality 10-30%. The lower left graph shows centrality 30-60% with R_{AA}. The bottom right graph shows R_{AA} for all other centralities.

Figure 6.3 shows R_{AA} for this analysis as a function of transverse momentum compared to negative kaons. The blue asterisks indicate the data from this analysis.

The value of N_{part} for the $Cu + Cu$ minimum bias data set is 35, which is equivalent to the 30-40% centrality bin. Comparison of the results in the analysis should fall roughly between the upper right panel and the lower left panel for Konno et al (K^- Figure 6.3, K^+ Figure **??**, π^- Figure 6.4, π^+ Figure **??**) [20].

The Nuclear Modification Factor (R_{AA}) for pions compared to R_{AA} for kaons is apparently inconsistent. That demonstrates that there could be a systematic error in the data not accounted for. Apparently, pions are more suppressed at high p_T than kaons; therefore, in R_{AA} for the $Cu + Cu$ analysis, the K/π ratio may be larger.

For stopped hadrons, negatively particles are dominated by particles that were originally pions since 70% of stopped hadrons are pions. Because K^- and π^- are different, an improvement for this measurement in the future would be to adjust the input ratios in the hadron cocktail.

This result appears to confirm the BRAHMS result (Figure 1.4) that the R_{AA} for hadrons is relatively independent of rapidity. This is a challenge for theoretical models predicting that the energy loss of particles should be proportional to the energy density since we expect that the energy density, at y=1.5, is (approximately a factor of 2) less than the energy density at y=0. All of these models predict R_{AA} to have a significant dependence on the energy density.

Due to the results collected over a number of years at RHIC and the theoretical interpretations, it is now generally accepted that partons propagating in quark matter lose energy mostly through medium-induced emission of gluon radiation.

6.2 Assisting the Field

How does this help the field of heavy ion physics? Although R_{AA} is not a direct probe for studying the QGP, these results can now be added to the catalog of results and presented as further evidence to help characterize the produced nuclear medium, the QGP. It may also lend some use for help in identifying the much sought after QGP critical point. Hopefully, these results will be used by future scientists to make further breakthroughs in relativistic

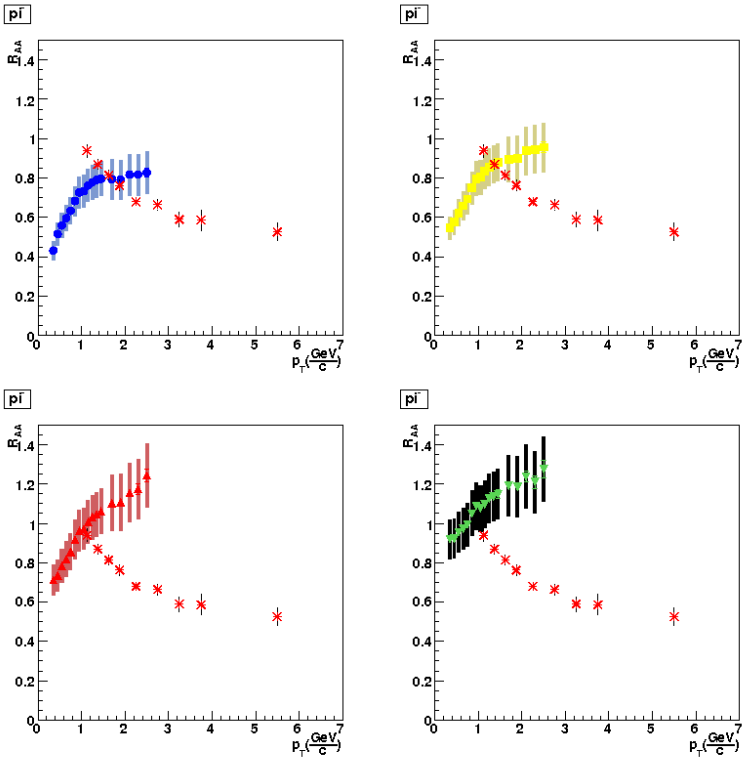

Figure 6.4: Transverse momentum distribution of R_{AA} for unidentified hadrons from this analysis (blue asterisks for $Cu + Cu$ data) with Konno et al. π^-. [20]

heavy ion physics.

References

Bibliography

[1] M. Riordan and W. A. Zajc, Scientific American, **May**, 2 (2006).

[2] E. Shuryak, Phyics Reports **61**, 1 (1980).

[3] hadronphysics.infn.it, Phase diagram of strongly interacting matter (artistic view), `http://hadronphysics.infn.it/course/view.php?id=8&topic=1`, 2008.

[4] J. Ritman, Pramana **66**, 857 (2006).

[5] M. Tannenbaum, Reports on Progress in Physics **69**, 2005 (July 2006).

[6] PHENIX, K. Adcox *et al.*, Nucl. Phys. **A757**, 184 (2005), nucl-ex/0410003.

[7] P. Stankus, "the short case for measuring hadron r_{AA} in the phenix muon arms and other forward detectors", Private Communication.

[8] C.-Y. Wong, (2007), 0712.3282.

[9] D. Hornback, "a measurement of open charm using single muons at forward angles for p+p collisions at center of mass energy 200 gev", Ph.D. thesis, 2008.

[10] BNL, Picture of the rhic facility (god's eye view).

[11] PHENIX, A. Adare *et al.*, Phys. Rev. Lett. **97**, 252002 (2006), hep-ex/0609010.

[12] H. A. et al., Nuclear Inst. and Methods in Physics Research A **499**, 537 (2003).

[13] K. A. et al., p. 489 (2003).

[14] M. L. Miller, K. Reygers, S. J. Sanders, and P. Steinberg, Ann. Rev. Nucl. Part. Sci. **57**, 205 (2007), nucl-ex/0701025.

[15] C.-Y. Wong, *Introduction to High-Energy Heavy-Ion Collisions* (World Scientific, P.O. Box 128, Farmer Road, Singapore 9128, 1994).

[16] PHENIX, S. S. Adler *et al.*, Phys. Rev. Lett. **94**, 082301 (2005), nucl-ex/0409028.

[17] P. R. Bevington and D. K. Robinson, *Data Reduction and Error Analysis for the Physical Sciences, Third Edition* ("McGraw-Hill Higher Education", 1221 Avenue of the Americas, New York, New York 10020, 2003).

[18] L. Hernquist and N. Katz, Particle Data Handbook **70**, 419 (2008).

[19] T. V. Cianciolo, Private Communication (2000).

[20] M. Konno, Private Communication (2008).

Vita

Dwayne John was born on December 18, 1982. In the spring of 2006, he completed his undergraduate career at Adelphi University with a B.S. in Physics. He matriculated at the University of Tennessee the following fall and graduated with the Master of Science degree in High Energy Nuclear Physics in the spring of 2009.